ISSN 0016-8521, Geotectonics, 2024, Vol. 58, No. 2, pp. 149–176. © Pleiades Publishing, Ltd., 2024.

Active Faults of Northern Central Mongolia, Their Correlation with Neotectonics and Deep Structure of the Region

V. G. Trifonov[a, *], S. A. Sokolov[a, b], A. N. Ovsyuchenko[a, c], S. Yu. Sokolov[a], Ts. Batsaikhan[d], S. Demberel[d], Yu. V. Butanaev[e], and N. G. Koshevoy[c]

[a] *Geological Institute, Russian Academy of Sciences, Moscow, 119017 Russia*

[b] *Russian State Geological Prospecting University named after Sergo Ordzhonikidze (MGRI), Moscow, 117997 Russia*

[c] *Schmidt Institute of Physics of the Earth, Russian Academy of Sciences, Moscow, 123242 Russia*

[d] *Institute of Astronomy and Geophysics, Mongolian Academy of Sciences, Ulaanbaatar, PO 13343 Mongolia*

[e] *Tuvinian Institute for Exploration of Natural Resources, Siberian Branch, Russian Academy of Sciences, Kyzyl, Republic of Tyva, 667007 Russia*

**e-mail: trifonov@ginras.ru*

Received February 22, 2024; revised March 14, 2024; accepted April 24, 2024

Abstract—The active tectonics of northern Central Mongolia is studied between two largest W–E-trending left lateral fault zones: the Khangai Fault and the Tunka–Mondy. These strike-slip zones are part of a single ensemble of active faults in the Mongol–Baikal region, formed under conditions of maximum northeastern compression and maximum northwestern extension. Their ENE-trending Erzin–Agardag and Tsetserleg faults with a dominant sinistral component extend between these zones. A series of the N-trending graben basins (Busiyngol, Darkhat, and Khubsugul) are located between the eastern end of the Erzin–Agardag strike-slip fault and the western part of the Tunka–Mondy strike-slip zone. The basins form a sinistral deformation zone, which is kinematically similar with the strike-slip faults, which follow the latter. In contrast to the largest boundary strike-slip faults, this structural paragenesis formed under conditions of N–S-trending relative compression and N–S-trending extension. A change in the orientation of the axes of the principal normal stress may be caused by the rotation of the block between the boundary faults. The area of graben-shaped basins is located above the top of a vast volume of low-velocity mantle, which we have identified as the Khangai plume. The lithospheric mantle above this rise is reduced; the remaining part of the lithosphere is heated and softened. The large active strike-slip faults are located above areas of subsidence of the low-velocity top of the mantle. Our trenching of the active faults showed that strong earthquakes repeated in the area of graben-shaped basins more often than in the large strike-slip zones, but they were characterized by lower magnitudes.

Keywords: active fault, strike-slip fault, neotectonics, trenching, paleo-earthquake, recurrence of strong earthquakes, mantle with reduced *P*-wave velocities

DOI: 10.1134/S0016852124700109

INTRODUCTION

The studied region spans northern Central Mongolia and neighboring areas of Southern Russia: the Khangai Highlands, the mountain systems of Eastern Tyva and Cis-Khobsgol, the southern slopes of the East Sayan, the Tunka and Ubsu-Nur basins and the Great Lakes Depression (Fig. 1).

The elevation of the relief varies from 4000 m in the south of the Khangai Highland to 700–750 m in Tunka and Ubsu-Nur basins. At the same time, throughout a significant part of the territory, except for Southern Siberia and Mongolian Altai, the relief is noncontrasting due to its relatively weak dissection.

In the west of the Khangai Highlands, outcrops of the Precambrian basement, which underwent Early Paleozoic tectonomagmatic reworking, dominate; to the east, Early Paleozoic folded-thrust complexes dominate. They are relics of the Paleoasian Ocean, which developed from the Late Precambrian to the Early Paleozoic [22]. The crust was consolidated near the Silurian–Devonian boundary; in the eastern part of the highlands it was affected by the Late Paleozoic and Early Mesozoic tectono-magmatic reworking due to impact of the Mongol–Okhotsk Ocean.

Continental conditions established in the considered region since the Late Paleozoic and Early Mesozoic. In the Jurassic and Early Cretaceous, there was a structural relief, the formation of which in the east of the region can be associated with the closure of the Mongol–Okhotsk Ocean. The Khangai Highlands was a provenance area of clastic material since the Jurassic. This is evidenced by Jurassic coarse-grained proluvial-type deposits in the Khan-Khukhiy Ridge north of Lake Khirgis-Nur. The transportation of clas-

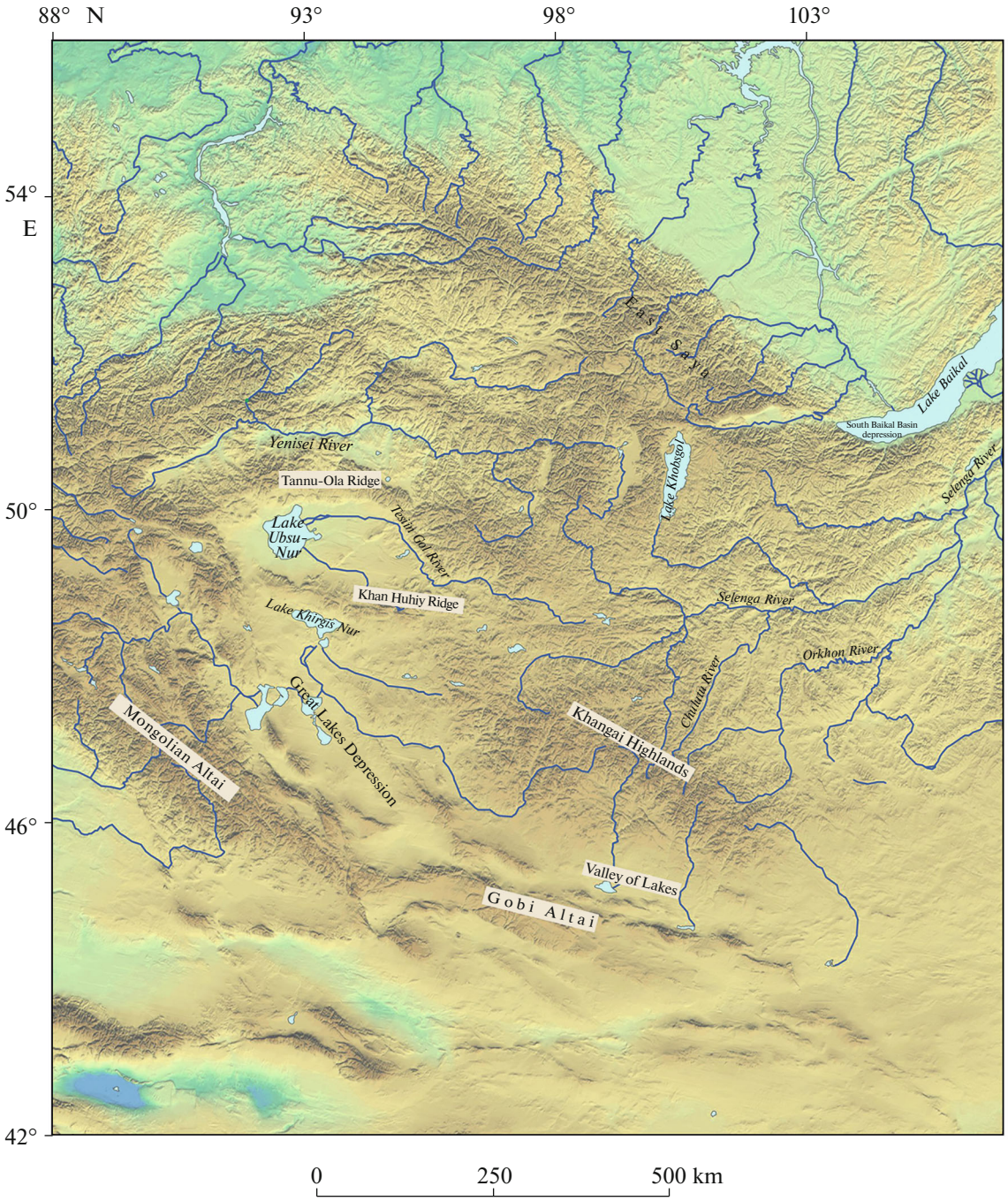

Fig. 1. Topographical map of Western and Central Mongolia and adjacent part of Southern Siberia.

tic material from the Khangai Highlands in the Jurassic and Early Cretaceous is also evidenced from the composition of deposits filled the early grabens of Transbaikalia [2].

The period from the Late Cretaceous to Early Oligocene was characterized by planation and relatively weak tectonic movements; the peneplain was partially covered by weathering crust [17, 21]. In the considered region, a denudation peneplain with the relicts of more ancient relief was formed, while to the south, in Gobi Altai and neighboring depressions and plains, an accumulative peneplain with a thin cover of fluvial and lacustrine deposits formed [8, 9]. At the same time, intensive subsidence of the South and Central Baikal basins occurred [16, 35].

The main features of the regional neotectonics were formed from the Late Oligocene and Neogene (Fig. 2).

The Khangai Highlands were formed as an isometric dome-shaped structure, elongated in the N–S direc-

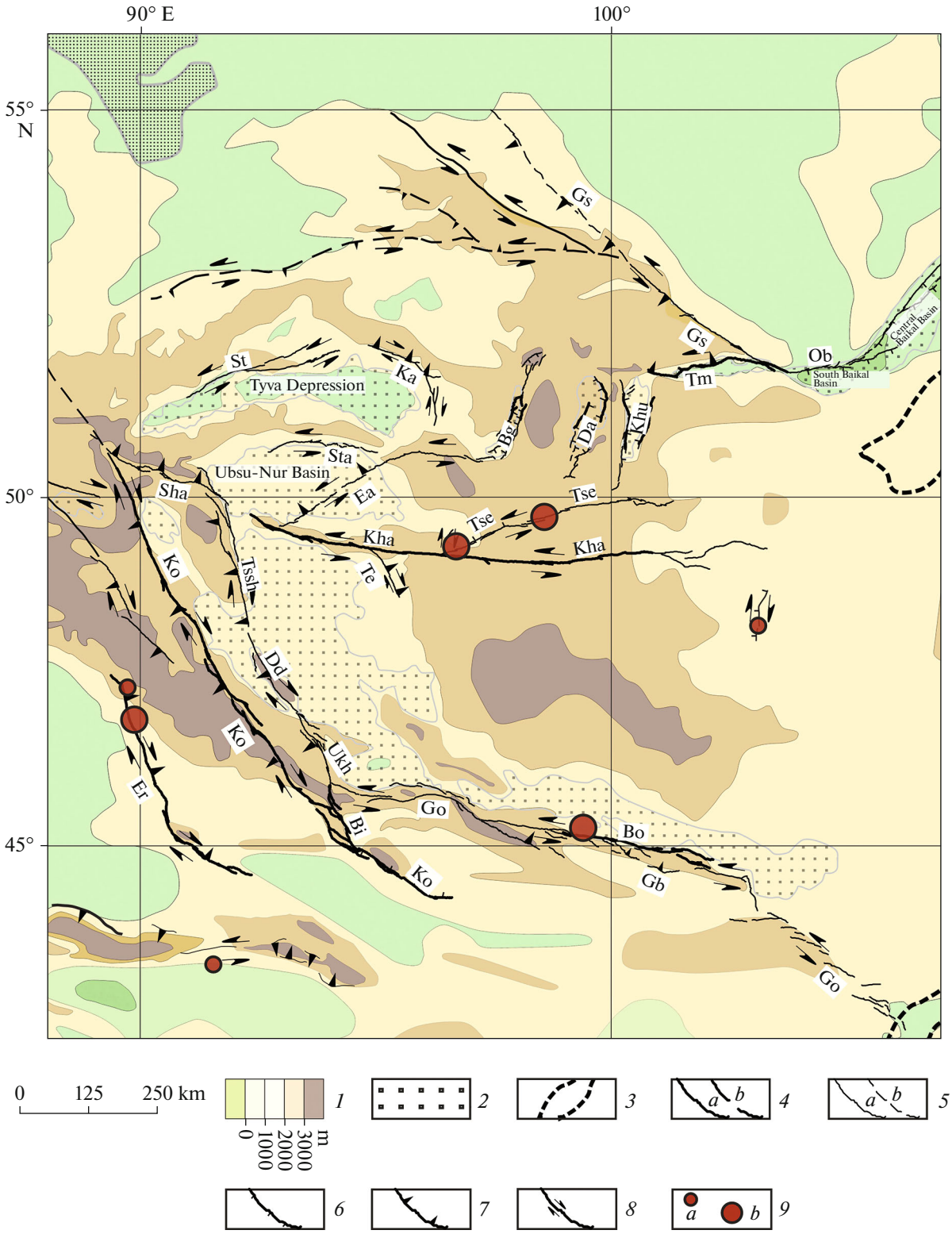

Fig. 2. Neotectonic map of northern Central Asia. *Active faults*: Bi, Bidj; Bo, Bogd; Gb, Gurvan-Bulag; Ms, Main Sayan; Dd, Dzun-Dgirgalant; Ko, Kobdo; Ob, Obruchev; St, Sayan–Tuva; Te, Teregtiin; Ukh, Umusion-Khairkhan; Kha, Khangai; Tssh, Tsagan-Shibet; Tse, Tsetserleg; Sha, Shaptal; Ea, Erzin-Agardag; Er, Ertai; Sta, South Tannu-Ola; *Fault zones*: Go, Gobi-Altai; Ka, Kaakhem; Tm, Tunka-Mondy; *Grabens*: Bg, Busyngol and Belin, Da, Darkhat, Khu, Khobsgol. (*1*) Summit plane of the basement surface on uplifts and the cover bottom in depressions (m); (*2*) sedimentary and volcanic filling of Cenozoic basins and grabens; (*3*) boundaries of linear troughs, Selenga–Vitim and southeastern Mongolia; (*4–8*) active faults: (*4*) major faults with displacement rate of ≥1 mm/yr: (*a*) confirmed, (*b*) inferred; (*5*) other faults with displacement rate of <1 mm/yr: (*a*) confirmed, (*b*) inferred; (*6*) normal faults; (*7*) thrusts and reverse faults; (*8*) strike-slip faults; (*9*) epicenters of earthquakes with magnitudes: (*a*) $M_s = 7–7/9$, (*b*) $M_s \geq 8$.

tion, most elevated in the south and lowered towards Cis-Khobsgol in the north. A C-shaped belt of intermontane basins, including the Tunka and Tuva basins in the north, Ubsu-Nur Basin and the Great Lakes Depression in the west, and the Valley of Lakes in the south, formed around the Khangai Highlands. The thickness of Cenozoic deposits that had accumulated since the Upper Oligocene increases to the north from 370 m in the Valley of the Lakes, 500 m in the Great Lakes Depression, and 700–800 m in the Ubsu-Nur Basin, to 2400–2500 m in the Tunka Basin [8, 20, 25, 65].

Linear fold-and-block uplifts of East Sayan, Tuva, Mongolian, and Gobi Altai were formed on the outer side of the belt of basins. Smaller linear uplifts developed between the belt of depressions: the Tannu-Ola Ridge between the Tuva and Ubsu-Nur basins and the Khan-Huhiy Ridge between the Ubsu-Nur Basin and the Great Lakes Depression. The significant similarity between the Upper Miocene sections on the northern slopes of the Ubsu-Nur Basin and the Great Lakes Depression makes it possible to suggest that they were deposited in a single sedimentary basin. This means that there was still no extended Khan Huhiy Ridge, which formed later, in the Pliocene–Quaternary.

The increased heterogeneity of the relief in the Pliocene is indicated by the occurrence of coarser fluvial deposits in the marginal parts of the Great Lakes Depression [8]. The uplift of the Khangai Highlands in Pliocene–Quaternary is also evidenced by the stairway of terraces up to 250 m high in the Selenga, Chulutu, and Orkhon river basins that cut into the northeastern slope of the highlands.

In the Pliocene–Quaternary, a network of active faults was formed in Central Mongolia [31, 32, 37, 46]. Most faults with signs of Late Pleistocene–Holocene activity are structurally interconnected and can be interpreted as elements of a single system of deformations caused by the interaction of lithosphere blocks. Some elements of this system are inherited from earlier stages of development up to the Paleozoic. However, faults as an integral system became pronounced only since the Early Pleistocene. Active faults limit and crosscut various elements of the neotectonic structure. The predominance of a strike-slip component in faults is a common feature of the fault system.

Northern Central Mongolia is bounded by two major W–E-trending sinistral strike-slip zones, the Khangai in the south and Tunka–Mondy in the north (Fig. 2), with the Erzin–Agardag and Tsetserleg active faults between them. In the north of the region, there are three N–S-trending grabenlike depressions (from west to east): the Busiyngol Basin, which continues to the north as the Belina, as well as the Darkhat and Khobsgoll basins, the marginal faults of which also bear signs of Late Quaternary activation.

The present paper aims to characterize the major active faults of the region between the Khangai and Tunka–Mondy zones of active sinistral strike-slip faults and determine their relationships and correlations with the neotectonic and deep structure of the region.

MATERIALS AND METHODS

To determine the location, structural pattern, and kinematic parameters of active faults and fault zones, the published data, including those presented in [51], were refined using remote sensing data and detailed elevation models created on their basis. More accurate data on some of the known faults were obtained and new faults were identified during field work using unmanned aerial vehicles (quadcopters) such as DJI Mavic Air Pro 2.

Recent seismic ruptures associated with earthquakes of 20th–21st centuries, amplitudes and directions of earlier displacements along the faults, geologic and geomorphologic position of the displacements were determined in the field.

To study the structure of seismic ruptures induced by earthquakes of 20th–21st centuries, as well as to identify and parameterize paleoearthquakes, trenching was carried out in the Tsetserleg and West Khobsgol fault zones and in the south of the Darkhat–Khobsgol interdepression bridge in the valley of the Belemiyn-Gol River. In addition, the previously obtained data on paleoearthquakes in the Khangai fault zone were reinterpreted [30].

Radiocarbon dating of 16 samples of carbonaceous deposits collected in the fault zone were performed in the Laboratory of Isotope Geochemistry and Geochronology of the Geological Institute of the Russian Academy of Sciences (Moscow, Russia) (analyst M.M. Pevzner). The conversion of laboratory dates into calendar ones was performed using the OxCal software [48] based on the IntCal13 calibration curve [60]. Samples of carbonaceous deposits collected during the field works in 2021–2022 were studied in the laboratory of the Institute of Archaeology and Ethnography of the Siberian Branch of the Russian Academy of Sciences (Novosibirsk, Russia). The calibration of radiocarbon ages obtained was performed on the basis of the IntCal20 calibration curve [61].

A structural map of the roof of the Khangai plume was compiled from the $\delta Vp = -0.5\%$ isosurface based on the MITP08 velocity model [55].

ACTIVE FAULTS IN THE STUDY AREA

Khangai (Bolnai) Fault Zone

This zone extends for a distance of more than 500 km, crossing the Khangai Highlands and continuing westward along the Khan Huhiy Ridge (see Fig. 2). In the west, the fault zone is adjacent to the Tsagan–Shibety N–NW-striking obliquefault (dextral with reverse component), which is the northern fault in the

eastern active fault zone of Mongolian Altai. In the Khangai fault zone, numerous Quaternary sinistral strike-slip displacements of landforms with amplitudes ranging from a few meters to 4 km were detected [32].

The conjugate Khan Huhiyn (Teregtiyn) according to [64]) dextral oblique-slip fault 80 km long departs from the Khangai Fault in the southeastern direction. The conjugate Bayan-Dungan dextral strike-slip fault follows from the area of convergence of the Khangai Fault with the Tsetserleg fault to the north and further to the north-northeast being traced for a distance of 34 km.

The strong Bolnai earthquake occurred in the Khangai fault zone on July 23, 1905 ($M_s \geq 8$) [23, 36, 37]. The earthquake epicenter was located near the conjunction zone of the Teregtiyn and Khangai faults, seismogenic displacement propagated along the Khangai Fault laterally, more to the east than to the west [64] (Fig. 3).

The Bolnai earthquake induced sinistral displacements with amplitudes up to 5–6 m [6]. The activated part of the fault zone (about 375 km) has been studied in detail [32]. The seismic rupture usually coincides with the active fault zone or deviates from it by up to 20 m. The deviation increases to 0.7 km near Lake Bust Nur and to 1.7 km near Lake Urtyn Nur.

The seismic rupture is expressed either as a compact strike-slip fault, or as en echelon series of NE-striking extension fractures up to the first tens of meters long, or as a zigzag-shaped combination of such extension fractures with NW-striking hummocks and extrusion ramparts.

According to [32], the westernmost signs of the 1905 seismo rupture were found near the village of Tsagan-Khairkhan. The strike-slip amplitude rapidly increases to the east up to 2–2.5 m up to the junction with the Teregtiyn Fault near the village of Under-Khangai.

To the east of the junction, the strike-slip amplitude sharply increases to 3.5–4 m near Dzun-Khangai village. To the east, it reaches 5.5 ± 0.5 m and remained unchanged for 200 km until the fault crosses the Jarantayn Gol River valley.

Further east, the strike-slip amplitude decreases toward Lake Sangiin-Dalai-Nur. Then, 20 km east of the lake, the seismic rupture attenuates. Vertical displacements are variable and significantly smaller than lateral displacements. In most cases, the southern side is uplifted. Seismic ruptures are vertical or inclined toward the uplifted side not less than 75°. This is evidence of overthrust kinematics of the vertical displacement. Analysis of detailed satellite images showed that the total length of the segment of the Khangai Fault activated in 1905 reaches 388 km [50].

Simultaneously with the Khangai Fault, the Teregtiyn Fault with dextral displacements up to 1.5–2 m was activated in 1905. The vertical component of displacement is variable, but in most cases the northeast-

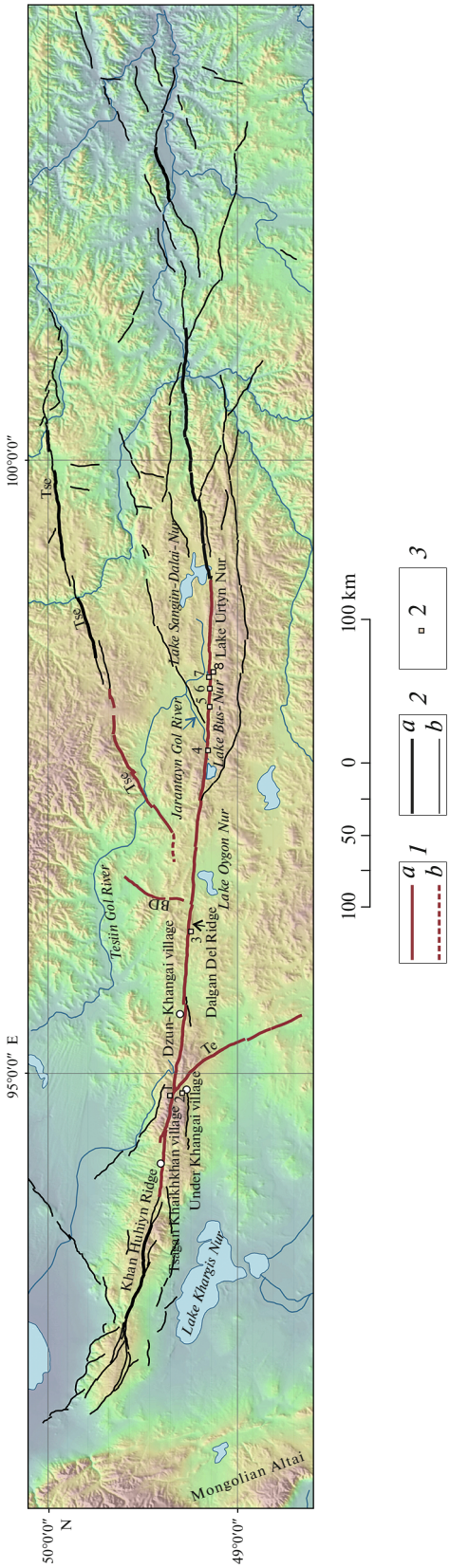

Fig. 3. Fragment of Khangai sinistral strike-slip fault, activated by 1905 earthquake. *En echelon faults*: BD, Bayan-Dungan; Te, Teregtiin; Tse, Tsetserleg. Arabic numerals: numbers of pits.

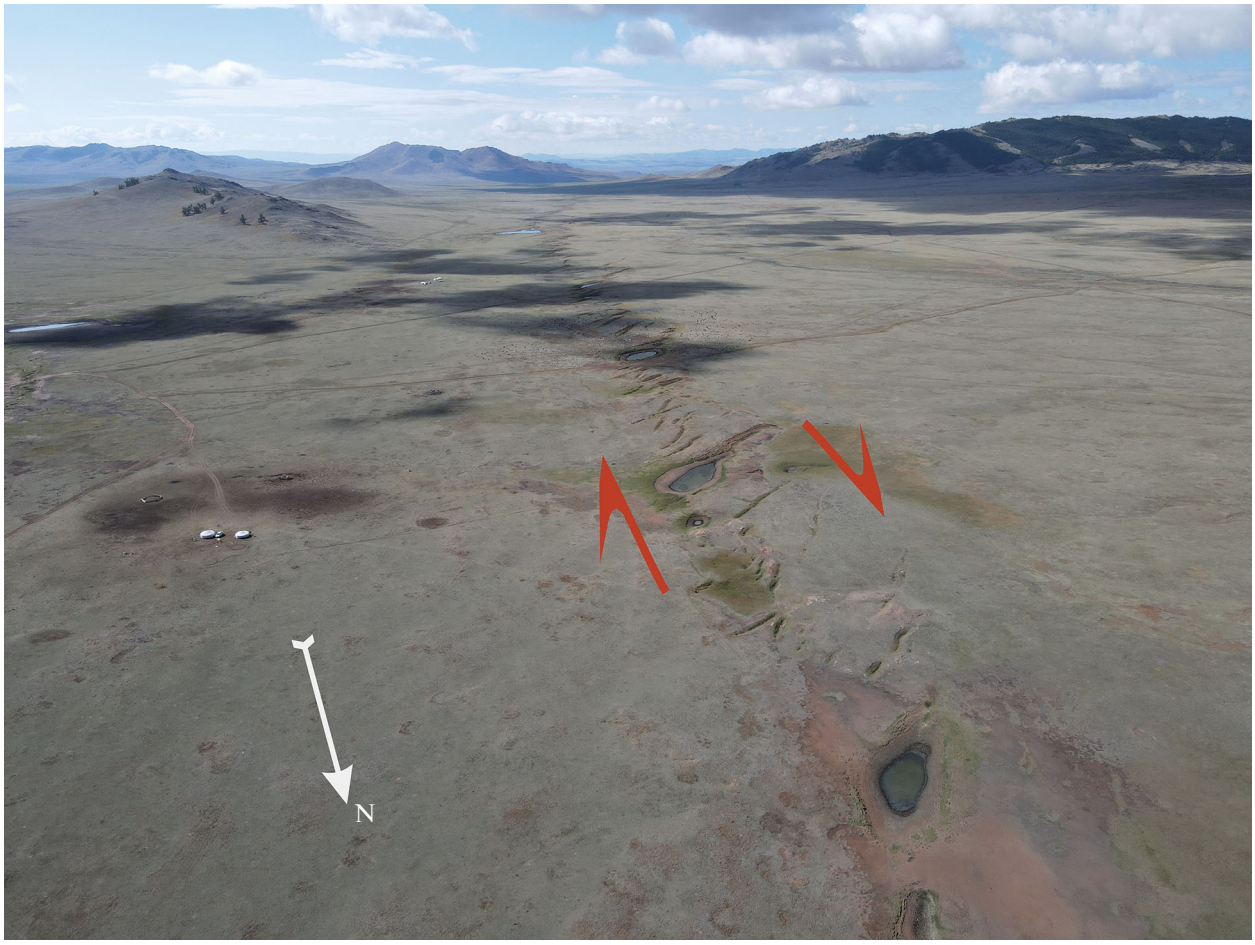

Fig. 4. Bayan-Dungan seismic rupture, 1905 year (photo from quadcopter).

ern wall is uplifted by 0.2–0.5 m. The fault is NE-dipping at angles of 65°–75°, indicating overthrust kinematics of vertical displacement. The 1905 slippage along the fault followed earlier displacements of the same kinematics.

The Bayan–Dungan fault is expressed on the Quaternary accumulative plain by a zigzag-shaped combination of nonextended extrusion ramparts and extension ruptures filled with latest deposits (Fig. 4).

The good preservation of these landforms suggests that it was also activated by the 1905 seismic events. The amplitude of the 1905 dextral strike slip is estimated at 0.3 m. Earlier 3.5–4-m strike-slip displacements, indicating recurring movements, have also been detected.

The first attempt at determining the average strike slip velocity along the Khangai Fault in Holocene was made in [30]. The revision of these materials made it possible to revise the estimates of the average velocity of Late Holocene lateral displacements and their correlations with strong earthquakes.

To identify paleoseismic events, we used the method proposed by R. Wallace [67] to identify displacements along the San Andreas Fault during the California earthquake of 1857. Wallace pointed out that there is a series of 9–12 m displacements related to this earthquake among the total number of small streams displaced along this faults. Larger amplitude maxima of displacements may be the result of the summation of displacements during the California and previous large earthquakes.

To apply such approach, the sections of the Khangai Fault to the southeast of Dzun-Khangai village were investigated in detail for a distance of 10 km and on the northern slope of the Dagan-Del Ridge for 15 km, where displaced streams and other landforms are especially numerous (see Fig. 3).

In total, 106 landforms displaced by up to 52 m were investigated in these sections of the Khangai Fault. It was revealed that the distribution of displacement values is irregular: 38 landforms were displaced by 5–6 m, obviously during the 1905 earthquake. Six more maxima of displacements as a multiple of this value were identified:

— ~11 m (3 landforms);

— 16–17 m (22 landforms);

— ~22 m (3 landforms);

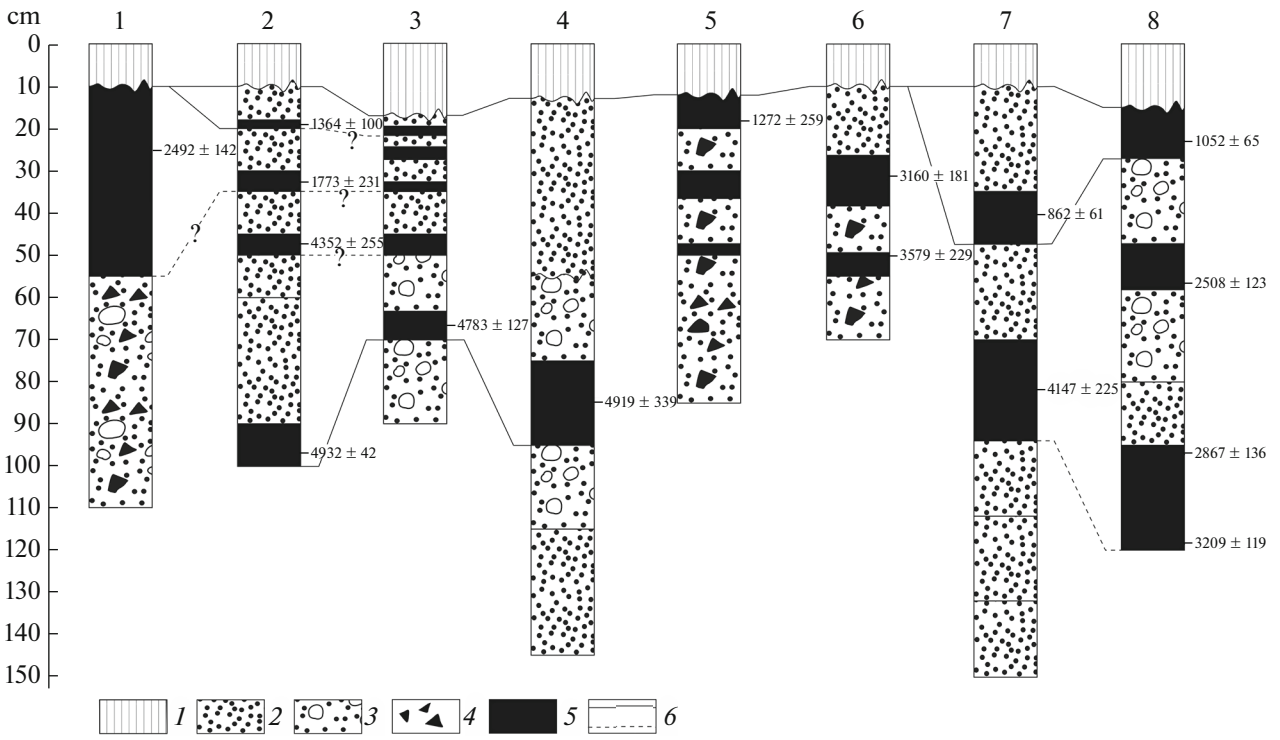

Fig. 5. Schematic sections of pits in Khangai Fault zone (after [30], modified). For position of pits, see Fig. 3. (*1*) Modern soil; (*2*) sandy-clayey deposits; (*3*) coarse debris; (*4*) rubble; (*5*) beds with carbon-bearing deposits; (*6*) correlation of beds.

— 28–29 m (7 landforms);

— ~33 m (5 landforms);

— ~39 m (5 landforms).

We interpreted these as a sequential buildup of total displacement by movement at another previous seismic event. The total displacement at the seven events being identified reaches ~39 m.

Tracing the 1905 displacement along the Khangai Fault showed that the seismic ruptures were located in en echelon relative to each other. Small pool-apart depressions filled with lacustrine-marsh deposits appeared between them. The damming of small streams due to seismogenic slip caused a similar effect. We suggested that such local depressions were created or deepened at strong earthquakes. In eight pits dug in the depressions, we found peat horizons (pit 1) or loam (all other pits) enriched with sapropel-type organic matter, which accumulated under lacustrine–bog conditions, probably after subsequent deepening of depressions during strong earthquakes (Fig. 5).

During the time intervals between the accumulation of these OM-bearing deposits, the depressions were filled with slope and deluvial detrital deposits. In addition, the flowal depressions were also filled with alluvial deposits. Sixteen radiocarbon dates of carbonaceous deposits were obtained (Table 1).

If calendar dates similar in age were obtained for the material from at least two pits, we interpreted the time intervals including these dates as upper age limits of paleoseismic events that caused deepening of depressions. Two dates obtained were excluded from consideration:

— no. 3290 in pit 2 because the uncertainty interval of the date was too large;

— no. 3296 in pit 6 because the date was not repeated in other pits.

As a result, we identified six time intervals that characterize strong paleoseismic events that caused deepening of depressions (Fig. 6).

When estimating the age of these seismic events, the location of radiocarbon sampling site within the carbonaceous horizon was taken into account. For event II, dates for two samples were obtained (see Table 1):

— 836 ± 60 BP for sample 3264 of pit 7;

— 1012 ± 58 for sample 3033 of pit 8.

The second date was obtained for the sample, which was collected closer to the lower boundary of the horizon and, accordingly, became preferable for dating. Sample 3032 taken from the upper part of the carbon-bearing horizon in pit 8 was not taken into account.

As a result of complex analysis of the obtained data, seven strong seismic events were identified. The ages of the paleoearthquakes may be slightly older than the radiocarbon dates because not in all cases the sample

Table 1. Results of radiocarbon dating (in years) of carbon-bearing horizons in sections of pits in Khangai Fault zone

Pit no.	Sample GIN RAS no.	Laboratory date, years	Calendar dates, calculated in 2023	
			date	date ranges
7	3264	920 ± 60 (1983)	836 ± 60	776–896
8	3033	1090 ± 50 (1982)	1012 ± 58	954–1070
5	3266	1300 ± 250 (1983)	1230 ± 255	975–1485
2	3288	1400 ± 100 (1983)	1318 ± 105	1213–1423
2	3290	1780 ± 200 (1983)	2020 ± 920	1100–2940
1	3293	2360 ± 100 (1983)	2443 ± 156	2287–2599
8	3262	2370 ± 80 (1983)	2461 ± 136	2325–2597
8	3032	2690 ± 110 (1982)	2809 ± 147	2662–2956
6	3297	2950 ± 150 (1983)	3118 ± 179	2939–3297
8	3265	2990 ± 90 (1983)	3160 ± 123	3037–3283
6	3296	3280 ± 180 (1983)	3526 ± 230	3296–3756
7	3034	3720 ± 160 (1982)	4094 ± 223	3871–4317
2	3291	3870 ± 180 (1983)	4298 ± 255	4043–4553
3	3274	4210 ± 80 (1983)	4726 ± 110	4616–4836
4	3035	4280 ± 250 (1982)	4865 ± 343	4522–5208
2	3295	4340 ± 20 (1983)	4902 ± 37	4865–4939

was taken at the lower boundary of the carbonaceous horizon. We believe, however, that these differences are insignificant.

As seen in Table 1, there were different time intervals between earthquakes:

— ~250 years (between events II and III);

— ~700 years (between events IV and V and events VI and VII);

— ~900 years (between events I and II);

— ~1000 years (between events V and VI);

— ~1200 years (between events III and IV).

Note that large time intervals preceded the events expressed by the largest number of displaced landforms, i.e., manifested over a significant extent of the fault zone. The average recurrence interval of strong earthquakes is ~800 years. Over the last ~5000 years, sinistral displacement accumulated by ~39 m, resulting in an average strike-slip rate of 7–8 mm/yr.

Later, the shear rate for a longer time interval was estimated at 2.5 mm/yr by the ^{10}Be method [63].

Tunka–Mondy Fault Zone

This zone bounds a chain of Tunka basins from the north: Mondy, Khoitogol, Tunka, Tora, and Bystrinskaya from west to east (Fig. 7).

The basins are separated by bridges, and the Bystrinskaya Basin is separated by the Kultuk bridge from the western end of the South Baikal Basin. Judging from the volcanosedimentary section of the largest Tunka Basin, the belt of basins developed from the Late Oligocene to the present. Geological and geomorphologic data available indicate the asymmetry of the depressions and the prolonged development of a fault zone with a normal fault component of displacements and a lowered southern flank along the northern side of the basins belt [17]. It is possible that this long-lived fault zone had a sinistral strike-slip component of movements. The active Tunka-Mondy fault zone follows this older zone.

Numerous left lateral displacements were detected along the Tunka-Mondy zone of active faults. The fault zone is segmented. The western segment is represented by the Mondy Fault, the western part of which is the northern boundary of the Khobsgol graben. In the west of the Khoitogol basin, the Mondy Fault is substituted from the north by the Tunka Fault, which in the east is adjacent to the southeastern segment of the Main Sayan Fault. The total length of the active fault zone exceeds 400 km. In the east this zone adjoins the active faults of South Baikal.

The strike-slip rate along the Mondy Fault was estimated at 1.1–1.5 mm/yr, with an thrust component rate of ~1 mm/year [4, 42, 49]. The subsequent detailed works within the Mondy depression [45] confirmed the uplift of the southern flank of the fault and the southward inclination of a fault plane at angles of 65°–75°. This is evidence of the presence of an reverse component of displacements opposite to the vertical displacement at earlier stages of development.

The sinistral slip rate has been determined as ~1.1 mm/yr. The uplift rate of the southern flank is

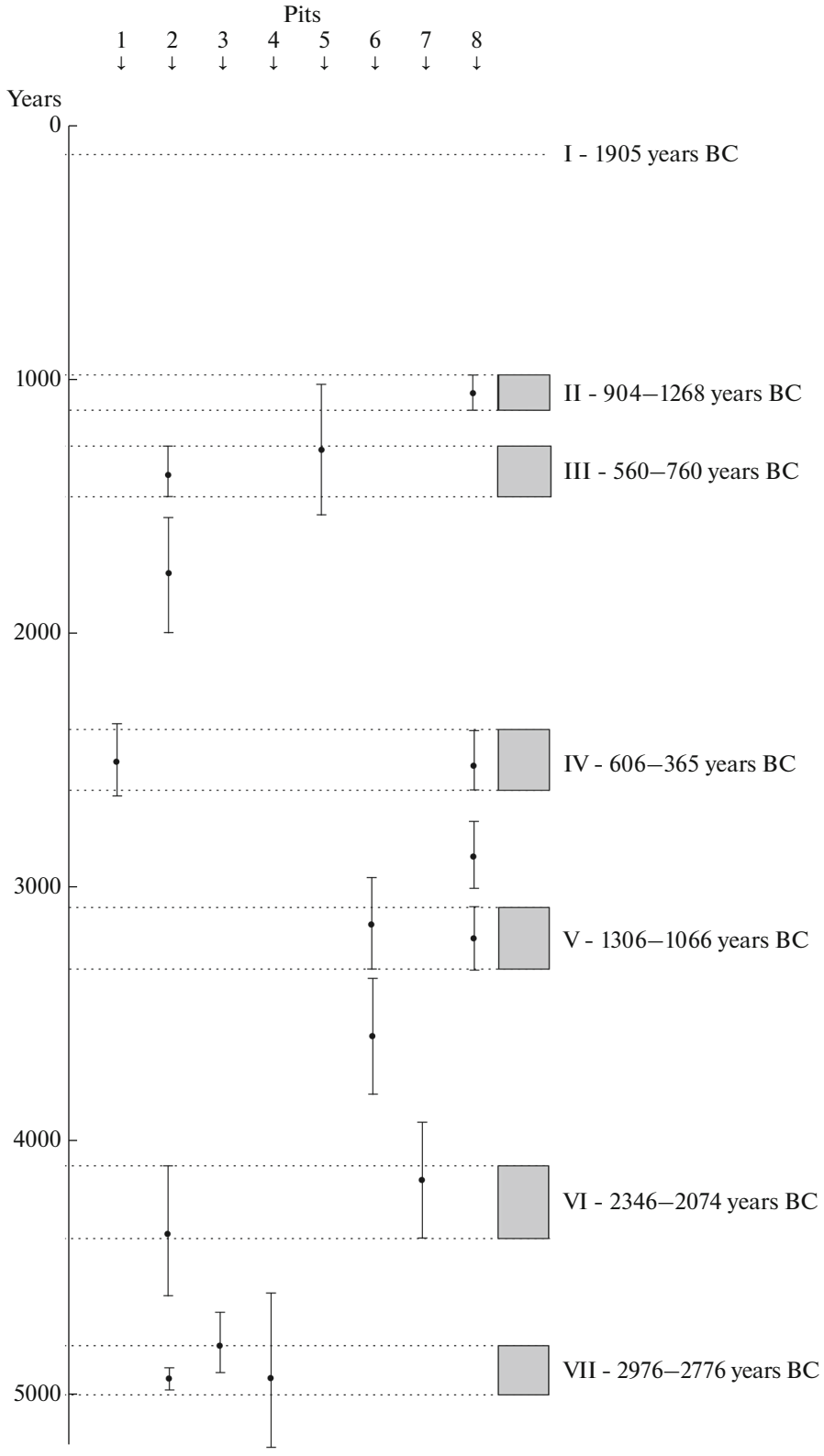

Fig. 6. Age intervals of strong paleoearthquakes II–VII, distinguished based on radiocarbon dating of deposits sampled in pits of Khangai Fault zone. For numbers of pits, see Fig. 5. Modern time scale (left); confidence intervals (Arabic numerals) of seismic events in calendar dates (right).

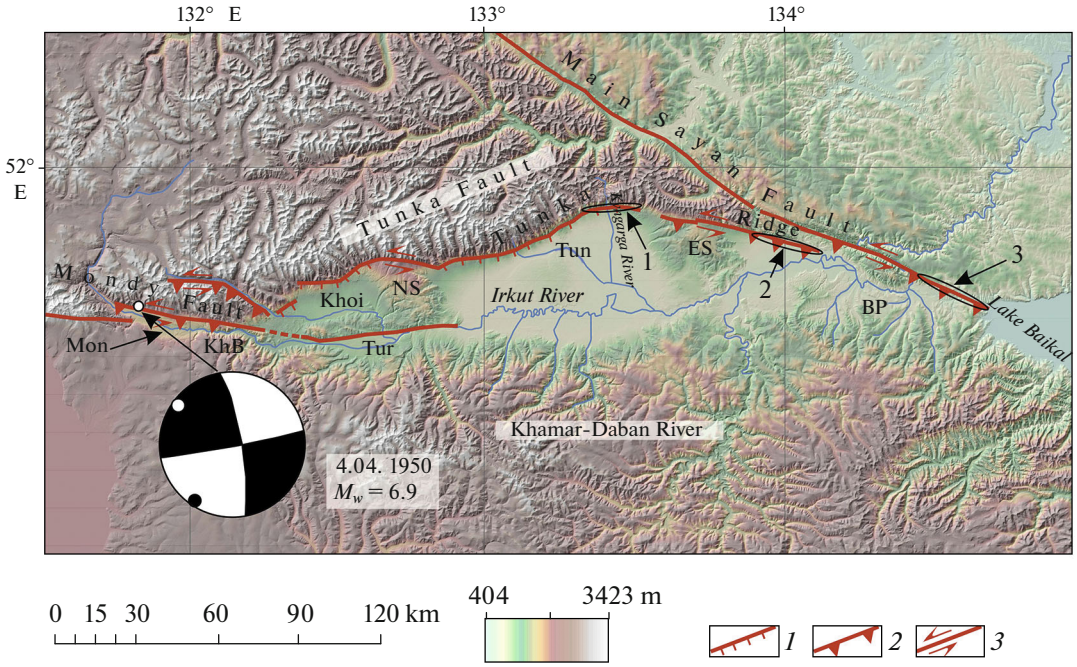

Fig. 7. Tunka–Mondy fault zone and Tunka system of depressions (after [45], modified). Lower hemisphere projection of focal mechanism of Mondy earthquake (1950) (after [52]); kinematics of faults (after [40, 41, 62]). *Depressions*: Mon, Mondy; Khoi, Khoitogol; Tun, Tunka; Tor, Tora; Bys, Bystrinskaya; *bridges*: KhB, Khara-Daban; BB, Bystrinskiy; *spurs*: NS, Nilovskiy; ES, Elovskiy. Paleoseismic dislocations (Arabic numerals): 1, Arshan; 2, Tora; 3, East Sayan. *1*, normal faults; *2*, thrusts and reverse faults; *3*, strike-slip faults.

~1.0 mm/yr; and that in the direction of the motion vector, ~1.5 mm/yr over the last 13 ka.

Along the Tunka Fault, the strike-slip rate increases to 1.5 mm/yr with a vertical component rate of 1 mm/yr [43]. In the most active southeastern part of the Main Sayan Fault, the sinistral rate reaches 1.4 ± 0.1 mm/yr and decreases northwestward of the junction with the Tunka Fault, passing to the latter [62].

The Mondy earthquake on April 4, 1950, with M_w = 6.9 occurred in the Mondy Fault zone. In the west of the Mondy fault, traces of three paleoseismic events with a recurrence interval of 4.1–4.6 ka were presumably identified, while in the east of the Mondy fault—traces of four seismic events with a recurrence interval of 3.9–4.3 ka [45].

Along the Tunka fault and in the southeast of the Main Sayan Fault traces of strong paleoearthquakes were found [26, 41]:

— Arshan paleoseismic dislocation (north of the Tunka Basin);

— Tora paleoseismic dislocation (north of the Tora Basin);

— East Sayan paleoseismic dislocation (in the southeast of the Main Sayan Fault).

In the Tora and East Sayan paleoseismic dislocations, traces of four strong seismic events with a recurrence interval of 3.9–4.2 ka have been revealed [62]. The correlation of paleoseismic events in different parts of the fault zone shows that they are similar in age within the accuracy of measurements. This suggests that during the last 13–14 ka the Tunka–Mondy zone has been activated throughout its entire length during the epochs of common seismic clusters [45].

Tsetserleg Sinistral Strike-Slip Fault

Although the Tsetserleg fault is en echelon relative to the Khangai Fault, no direct conjunction of these two faults is observed. The Tsetserleg Fault pronounced on the surface starts 21 km northeast of Lake Oigon Nur and follows northeastward and further eastward, crossing the Khangai Highlands and forming a northwestward-convex arc (Fig. 8).

The fault consists of three segments. Each more easterly located segment builds up en echelon a more westerly segment from the south. The substitution of the southwestern segment by the central segment occurs on the right (northern) side of the Tesiin Gol (Tes-Khem) River valley, where the ends of the segments are spaced 0.6–0.8 km apart. The Tsetserleg earthquake occurred within the fault zone on July 9, 1905. According to [64], its magnitude was M_w = 8.0, the epicenter was located in the southwest of the central segment, and seismic ruptures and displacements spread over 190 km more to the east than to the southwest.

We investigated the 130-km western part of the 1905 seismic rupture zone, covering the southwestern

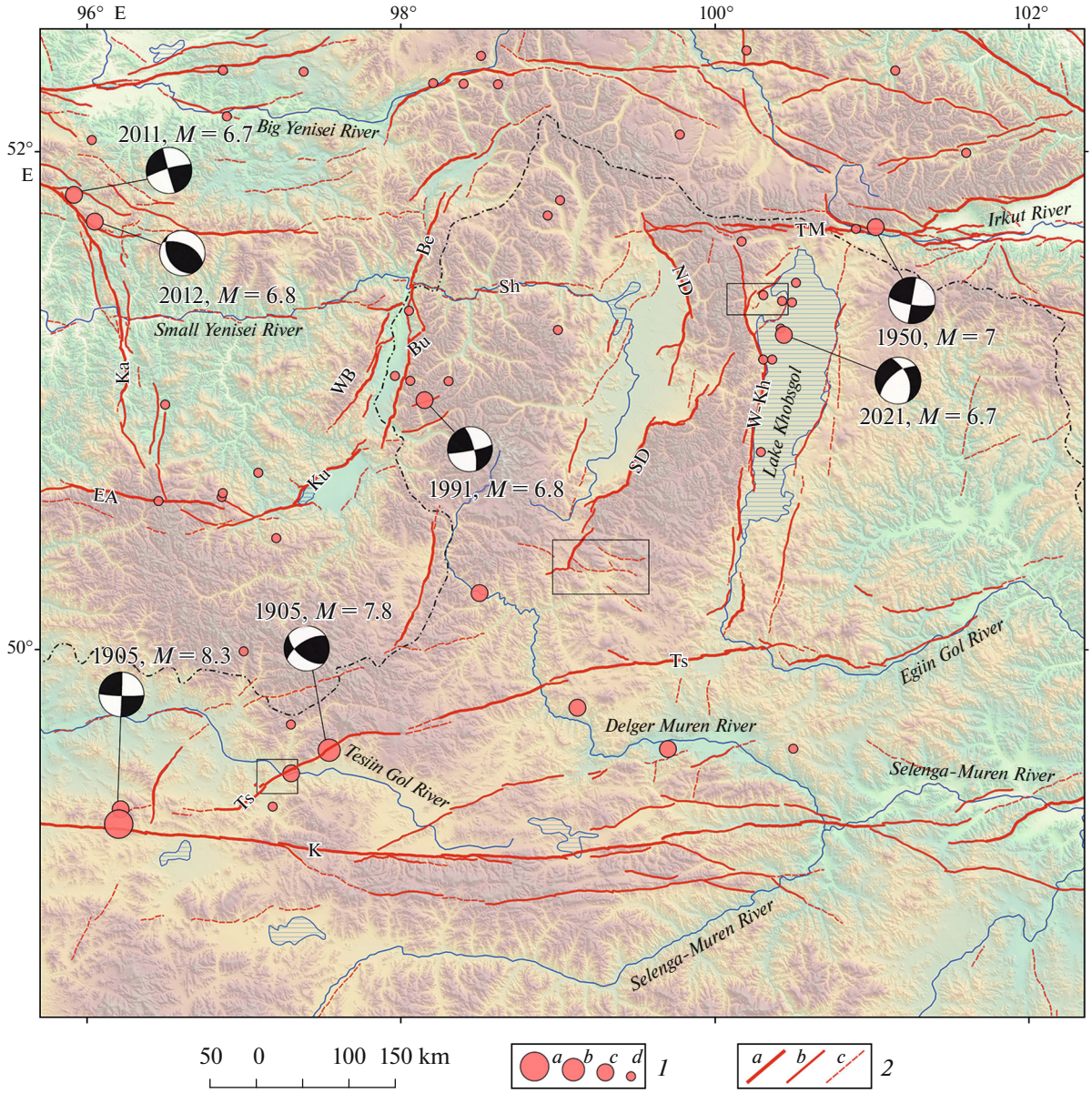

Fig. 8. Active faults, epicenters of strong earthquakes after 1900, and mechanisms of earthquake sources between Khangai and Tunka–Mondy zones of active strike-slip faults (after [51, 55, 59, 68], modified). *Main faults*: Kha, Khangai; Ts, Tsetserleg; EA, Erzin-Agardag; Ka, Kaakhem; Kz, Kyzylkhem; Be, Belna; Bu, Busiyngol; WB, West Busiyngol; Ky, Kungurtug: Shi, Shishkhidgol; Sd, South Darkhat; Nd, North Darkhat; WH, West Khobsgol; TM, Tunka–Mondy. Sites of detailed field works are outlined by rectangles. (*1*) earthquake epicenters with magnitudes: *a*, ≥8; *b*, 7.5–7.9; *c*, 6.5–7.0; *d*, <6.5; (*2*) active faults: (*a*) major (with average displacement rates ≥1 mm/yr), (*b*) moderate (<1 mm/yr), (*c*) minor.

and partially central segments of the fault zone. The southwestern segment extends along an azimuth of 50°–60° NE. The main seismic rupture is represented in most cases by en echelon series of extension trenches extending in an azimuth 20°–30° NE, or by a zigzag-shaped combination of trenches with mounds and squeezing shafts oriented along an azimuth of 285°–290° WNW [32].

The amplitude of the sinistral displacement reaches 3–3.3 m on the northeastern bank of the Tesiin-Gol River, where the fault plane is vertical. The roots of older larch trees within the seismic rupture zone were faulted and displaced during the earthquake. Younger larches show no signs of deformation that indicates no significant displacements after 1905.

In the central segment, the amplitude of the sinistral strike-slip fault at the 1905 earthquake is close to 2.5 m [37]. In both segments, the shear zone is accompanied by uplifting the northern sides of the seismic ruptures, which does not exceed 0.6 m in the south-

western segment and reaches 1.5–2 m in the central segment. In the area of the echelon substitution of the segments, the vertical displacement is variable. In some places, the southern sides of the seismic ruptures are upthrown, and short echelon series of extension fractures appeared south of the end of the central segment.

In the central segment of the Tsetserleg Fault, sinistral displacements of landforms with an amplitude of up to 124 m, apparently related to earlier displacements along the fault were detected. In the extreme east of the studied part of the fault (Ikhe-Bogdo-Ula Mountain and its environs), the seismogenic rupture divides into a number of low-amplitude scarps and extension fractures and becomes less expressive.

The maximum sinistral displacement was detected in 2022 at the intersection of the fault zone with the Tesiin Gol River valley, where the southwestern segment of the fault is substituted with the central segment. The accumulated displacement is expressed by two bends of the Tesiin Gol River channel along the two indicated segments (Fig. 9a).

The total amplitude of the displacement reaches 6.75 km. To the southwest, a left tributary of the Tesiin Gol River at the intersection with the Tsetserleg Fault is knee-shaped leftward for ~4 km. Upstream the crossing the valley widens considerably with signs of damming.

On the floodplain of the right bank of the Tesiin Gol River, the signs of the Tsetserleg Fault are partially veiled by recent fluvial erosion, accumulation, and permafrost processes and sediments of the Shavaryn Gol River, that is the right tributary of the Tesiin Gol River. The fault is traced by few echelon fractures, dry channels and bayou extending along the fault strike, and small wetlands confined to areas of extension in places where the fault line is displaced to the left.

Beyond the floodplain, the 1905 seismic rupture is more pronounced due to the occurrence of a system of extension fractures and compression shafts reflecting the sinistral kinematics of the strike-slip fault. In open areas, the fractures are filled with soil material and covered with relatively dense vegetation. The fractures in forested areas on slopes of northeastern exposure still look like the fresh gaping ditches.

On the left, southwestern, bank of the Tesiin Gol River, the Tsetserleg Fault crosscuts the terrace above the floodplain, the flat surface of which dips gently north-northeast to the high floodplain of the river (see Fig. 9b).

The terrace cover consists of slope and floodplain sandy–gravel deposits. In the northeastern part of the terrace, a fault extends along its rear side, at the base of a steeper eroded slope rising to the southeast. Dry channels of temporary streams incised into the terrace surface are displaced leftward along the rear-side line relative to their headwaters. The maximum displacement is 124 m, which reflects accumulated displacement along the fault. The minimum displacement of 4.8 m probably corresponds to the displacement amplitude of the 1905 earthquake.

The geomorphological records of this earthquake, represented by a set of characteristic landforms reflecting the sinistral slip kinematics, are well preserved. Along the rear side of the terrace, en echelon series of extension fractures forms a relatively narrow zone (~15 m) extending along the Tsetserleg Fault to the northeast along an azimuth of 55°–60°. The fractures extend along azimuths of 30°–50°, i.e., at angles of 5°–10° to 30° to the fault line. The cracks are up to 35 m in length and 1 m in depth.

Southwestward, the fracture zone is traced to the gently-dipping terrace surface, moving away from the rear side. As a result, the zone becomes less manifested. Here the width of the fracture zone increases to 40–45 m and their length increases, reaching 50–60 m in some cases. The orientation of the fractures becomes more consistent in the direction of 30° NE.

In this segment, a rupture up to 0.5 m deep stretches along the fault (along an azimuth of 60°) for 430 m. The southwestern end of the rupture rests on a the 85° ENE-trending reverse fault scarp. Its northern side, opposite to the general northern slope of the terrace surface is raised. The height of the scarp reaches 1 m.

To the north of the reverse fault scarp, the surface is complicated by numerous tension fractures, the length of which increases and can reach 120 m. There are also small extrusion ramparts in the disturbed zone.

To the southeast, a smoothed NE-striking scarp with a slightly uplifted northwestern side was identified on the erosion slope. Its poor preservation may indicate an older age and the manifestation of an earlier seismic event.

In 2022, we cut two trenches within the Tsetserleg Fault zone to detect traces of paleoearthquakes (Fig. 9c).

A trenching site was chosen at the rear side of the suprafloodplain terrace on the left bank of the Tesiin Gol River, about 30 km southwestward from the supposed epicenter of the 1905 earthquake according to [64]. The trenches were cut across the strike of two extension troughs expressed in the topography.

The first trench (T-1) was cut across the "fresh" 1905 trough. It is a symmetrical minigraben about 1.5 m wide in section view, filled with recent soil (up to 0.7 m thick). No traces of previous displacements were found.

The second trench (T-2) exposed a section of an older tilt, represented in relief by 20–30 cm-deep a linear depression and a ~20-cm high scarp. The trench was cut 2.5 m upslope above the 1905 rupture (Fig. 9c). The average surface tilt increases from 15° (linear depression) to 20° (scarp) and 25° (1905 trough). Probably, this is determined by three stages of faulting.

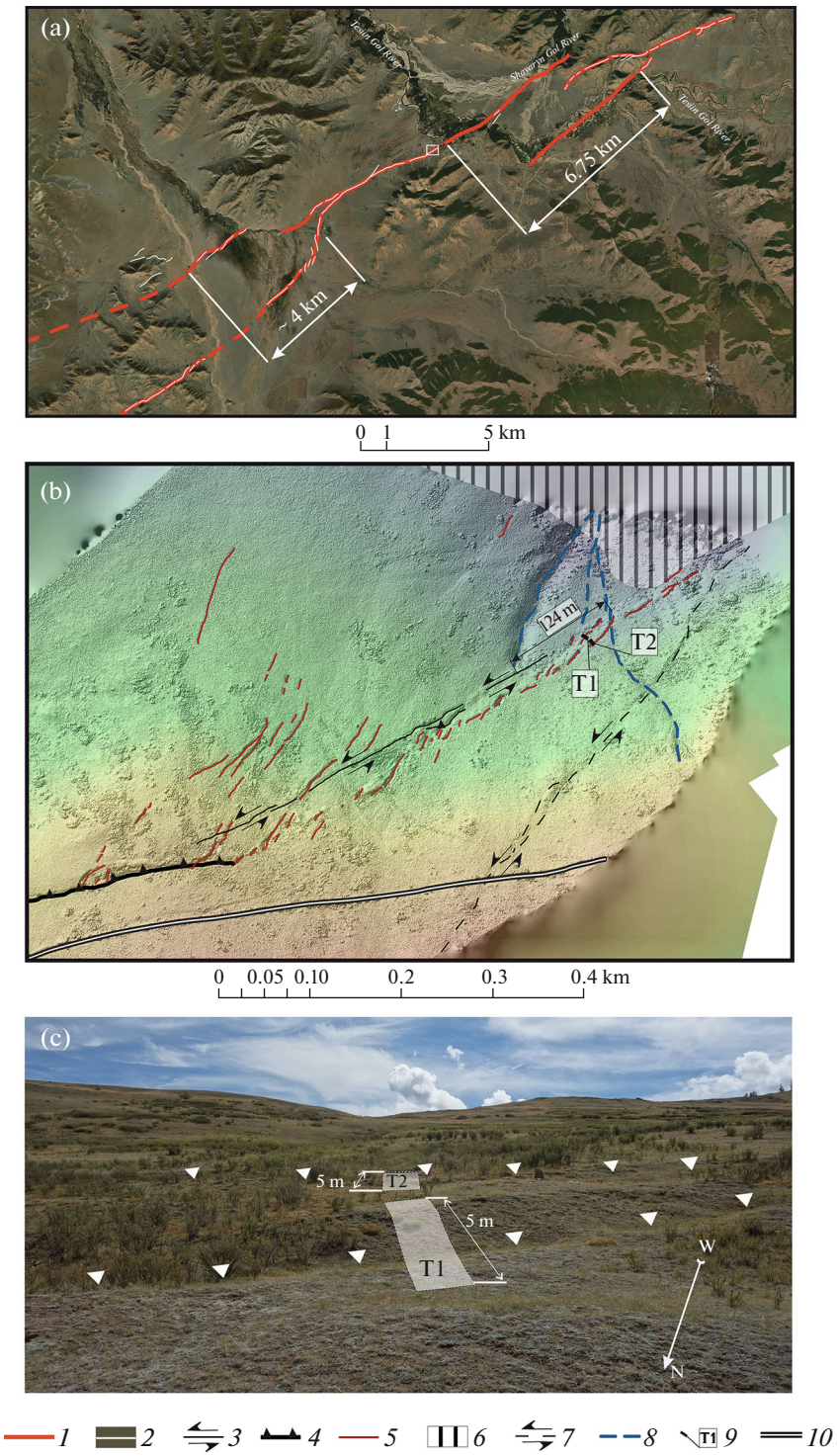

Fig. 9. Tsetserleg Fault in area of its intersection with Teisiin Gol (Tes-Khem) River Valley. (a) Structural scheme of Tsetserleg Fault (trenching site is shown by rectangle); (b) Tsetserleg Fault at trenching site; (c) general view of trenches T-1 and T-2. (*1*) Fault plane on surface; (*2*) traces of 1905 earthquake; (*3–5*) seismodislocation of 1905 earthquake: (*3*) strike-slip seismic trough, (*4*) reverse fault scarp, (*5*) extension fracture; (*6*) flood-plain; (*7*) ancient tectonic scarp; (*8*) thalweg of temporary water stream displaced by fault; (*9*) location of trenches; (*10*) road.

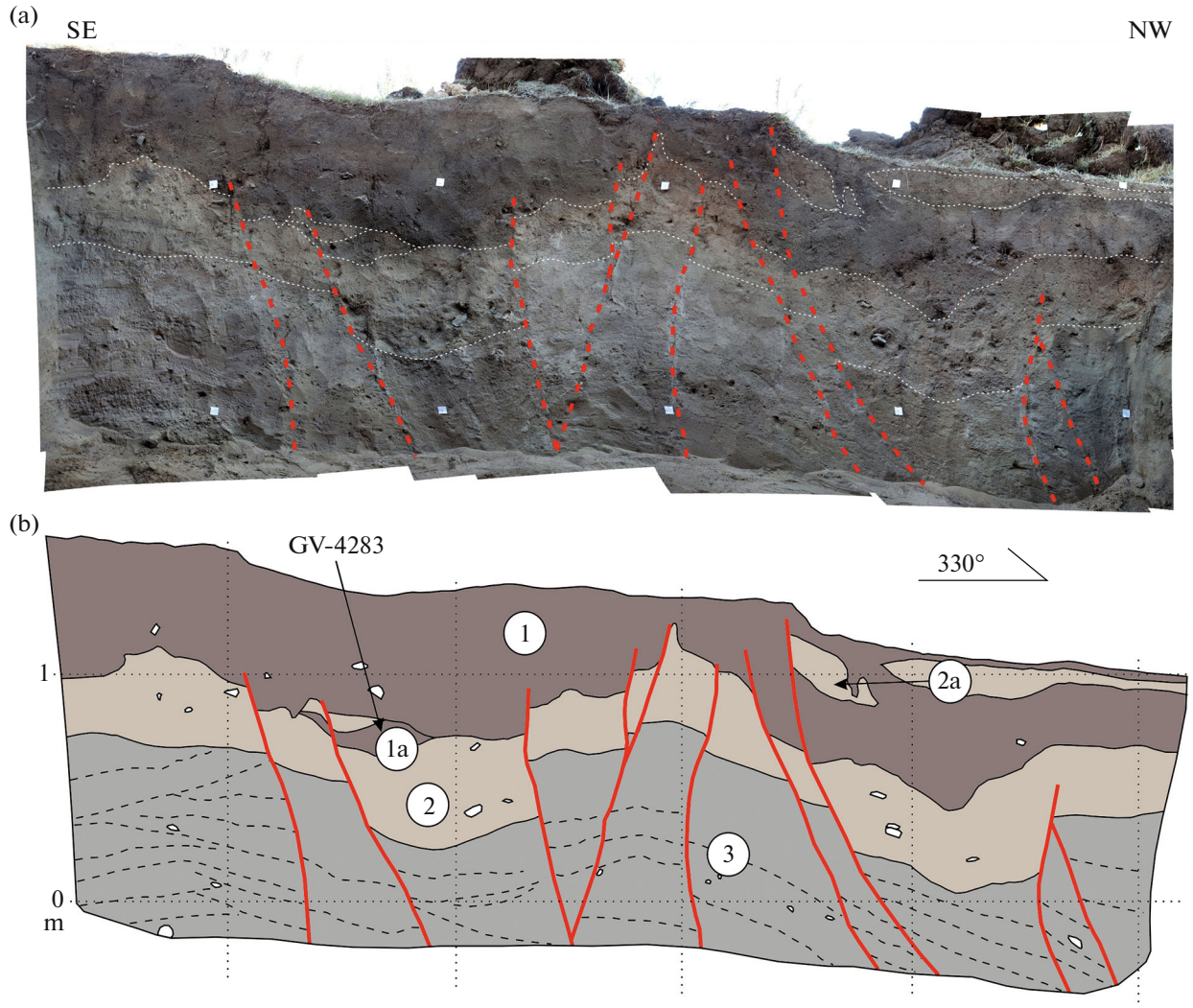

Fig. 10. Transverse trench T-2 of ancient trough in Tsetserleg Fault zone. (a) Photo of trench; (b) section of trench. Ruptures (red lines); layering of alluvial deposits (black dashed lines); sampling site for radiocarbon dating (GV-4283) are shown. Circled numbers: (1) steppe sandy brown soil (humic horizon), (1a) buried fragment of paleosol; (2) brown silt loams with lenses of gravel-gruss material and rare rubble (slope deposits), (2a) redeposited loams from same horizon; (3) cross-bedded alternation of well sorted silt sands with lenses of coarsely sorted sandy-gravel material (floodplain alluvium).

A linear trough was uncovered in the southeastern part of the trench, formed by counterdipping stepped normal faults (Fig. 10).

All layers of the exposed section dip stepwise. In the graben between the normal faults, the bottom of the recent steppe brown soil is subsided. This horizon is underlain by sands, which encloses a fragment of humus horizon of paleosol 1a (Fig. 10). A sample from the buried soil humus lens was taken for radiocarbon dating. A calibrated age of 3319–3506 years ago (the radiocarbon date of 3164 ± 35 years, laboratory code of the sample is GV-4283) was obtained for humic acids.

It can be assumed that the paleosol was buried as a result of seismotectonic movement, which led to the formation of the linear trough pronounced in the topography after the deposition of the soil layer of 3319–3506 year ago.

The younger scarp in the northwestern part of the trench is formed by stepped normal faults that form, the wall of an asymmetric graben. Its opposite side is less pronounced. However, here there is a bending rupture with vertical displacement of the base of slope deposits. In the upper part of the section the bottom of the recent steppe soil is observed. At the same time, part of the brown soil horizon was buried by redeposited slope sandy loam 2a, above which the sod horizon of recent soil accumulated (Fig. 10).

It can be suggested that traces of another displacement following the first one are recorded here. Thus, the trench opens traces of two different-age single-act displacements that occurred during the last 3319–3506 years and preceded the 1905 earthquake.

Erzin–Agardag Sinistral Oblique-Slip Fault

The Erzin-Agardag Fault stretches within the Ubsu-Nur Basin 240 km west of the Tsetserleg Fault (Fig. 8). It starts in the northern foothills of the Khan Huhiy Ridge and crosses the Ubsu-Nur Basin in the northeastern direction along an azimuth of about 60°, coinciding with the strike of the Tsetserleg Fault. Within the depression, the fault is traced for 240 km. It crosses its northeastern boundary, outlining the Ostrokonechny Ridge from the northwest. Further, the fault acquires a sublatitudinal strike and is traced to the southern end of the Terekhol Basin, which joins the Busiyngol graben zone [1].

Despite a number of studies [1, 27], neotectonic activity, movement rate, and cyclicity of seismic events along the Erzin-Agardag Fault have been poorly studied to date. Throughout its entire length, the fault bears sign of sinistral strike slip with a reverse component in some segments. Sinistral deformations is confidently established by the displacements of permanent and temporary streams along the surface outcrop of the fault plane.

The established minimum displacement amplitudes of stream channels identified in the Mount Khairakan area is 5–7 m, which is close to one-time displacements at the earthquake. Accumulated strike-slip displacements ranging from 280 m to 1.5 km are recorded in the northeast of the Ubsu-Nur Basin, along the knee of the Tesil Gol River (Tes-Khem) and the isolated fragment of slope of Mount Khairakan [1, 27].

The different segments of the Erzin-Agardag have been excavated by trenches in two places.

The first trench was cut in the southwest of the Erzin-Agardag Fault within the Khirgis-Nur Basin [1].

The second trench was cut in the northeast of the Ubsunur depression at the foot of Mount Khairakan [27].

The traces of seismic events and local minor vertical displacements are visible in both trenches. The main component of displacement is horizontal. The second trench opened a complex "flower" structure characteristic of the strike-slip kinematics of the fault and traces of several different-age seismic events.

The dry climatic conditions of the region do not favor the accumulation of deposits enriched with organic matter. Due to this, paleoearthquakes are difficult to date. Thus, there is still insufficient information for periodization of seismic events and estimation of fault velocity.

Busiyngol, Darkhat, and Khobsgol Grabens

The Cis-Khubsugul grabens form a the W–E-trending system of N–S-trending troughs separated by steep and high mountain massifs (see Fig. 8). These structural landforms are very contrast: Lake Khobsgol is as deep as 262 m, while the mountain massifs rise steeply 1500–2000 m above the depressions and represent typical highlands, often with alpine landforms. The knowledge of the sedimentary cover of these depressions is based on gravity, seismic, and drilling data [15, 34, 54, 57]. The Cis-Khobsgol troughs are filled with facies variable lacustrine, alluvial, proluvial, glacial, fluvioglacial, and aeolian deposits. The deepest well penetrated the sequence of the Late Pliocene–Quaternary lacustrine deposits in the Darkhat Basin to a depth of 211 m [15].

The sediment thickness, size, and morphological expressiveness of the Cis-Khobsgol troughs decrease from east to west with distance from the Baikal Basin. The thickness of the sedimentary cover in the depressions is as follows:

— 500–700 m (Khobsgol) [34];

— 450 m (Darkhat) [15].

The Busiyngol graben and the Belina graben located northward are slightly filled with sediments. Starting from 5.5–6 Ma, the formation of sediments of Lake Khobsgol marks the beginning of the neotectonic (late orogenic) stage [34]. The lacustrine deposits of this age overlie alluvial deposits and basalts dated to 9.5 Ma [58].

The spore–pollen date older than 4 Ma also provides insight into the lower age limit of the initial stage of the neotectonic activation in the Cis-Khobggol, when the existing sedimentation regime was violated and the exposed Pliocene strata became the object of denudation [10].

The onset of the late-orogenic tectonic stage is fixed by the latest stage of basaltic volcanism in the Lake Khobggol area (5–4 Ma), which was preceded by several stages of volcanic activity: 8–12, 12–16, and 18–22 Ma [58]. The age of the "valley" basalts is the Early Pliocene (4.93–4.18 Ma), in addition to the age of lava complexes of small shield edifices (5.84–5.10 Ma), allows us to presumably estimate the age of the onset of the emplacement of the Darkhat Basin as the Late Miocene–Early Pliocene [38].

The Busiyngol graben and continuing it to the north Belina grabens are considered the main magma-providing structure at the recent stage of volcanism in East Tyva [28]. This structure determines the location of almost all volcanic centers of the East Tyva lava highlands. The age of basaltic lavas here is considered the youngest for the Cis-Khobsgol Basin system: 2.8–2.1, 1.6, 1.2, 0.76–0.725, 0.6–0.56, 0.35–0.29, and 0.048 Ma [28].

On the western wall of the Darkhat Basin, basalt lava filled the Shishkhid Gol River valley and formed a well pronounced terrace. The height of this terrace is only a few meters, whereas within the adjacent mountain massif from the west, its height gradually increases to 80–90 m [10], fixing the absence of significant faults in the western side of the basin. The Miocene basalt plateau at the low, weakly deformed eastern side of the Khobsgol Basin has a similar structure [58]. This mor-

phology determines the pronounced asymmetry of the Khobsgol and Darkhat basins.

The Busiyngol Basin has a less clearly pronounced asymmetric structure, since the eastern tributaries of the Busiyn Gol River, unlike the western tributaries, are sharply bent when flow out of the mountain massif due to tectonic scarps of hanging valleys [5]. The reason of the asymmetry of the Busiyngol Basin is that its western side does not have such a sharp boundary as the eastern one. According to remote sensing data, the faults along the western side of the depression are characterized by smaller values of the Late Cenozoic displacements and form a series of relatively short (10–15 km) segments that cut glacial landforms and Holocene river terraces.

The Belina trough was described by V.V. Vdovin [5] as a narrower bilateral graben. The reason for its difference from the Busiyngol trough could be an active W–E-trending strike-slip fault separating these structures and tracing along the Kyzyl-Khem and Shishkhid Gol river valleys [5]. The frequent traces of cracks and rockfalls on slopes are considered traces of strong earthquakes.

Busiyngol Basin. A system of fault scarps as long as 20 km, which cut young cones and moraine deposits, was mapped along the eastern wall of the Busiyngol Basin based on aerial photographs [37].

The Busiyngol earthquake with $M_s = 6.5$ occurred on December 27, 1991, in the mountain frame to the east of this depression. This seismic event led to seismic activation in the region unique in duration and pulsating mode [11]. The focal mechanism is considered a strike slip, dextral on the N–NW-striking plane or more probable sinistral on the E–NE-striking plane.

According to the distribution of aftershocks, the earthquake focal zone is confined to the E-NE striking auxiliary fault adjacent to the Busiyngol depression at an acute angle. This fault continues en echelon to the north the Kungurtug active fault in the northern side of the depression of the same name, connecting the Belina–Busiyngol graben zone and the Erzin-Agardag Fault.

Darkhat Basin is the least seismically active structure over the last 100–110 years among the Cis-Khobsgol basins. At the instrumental stage of seismic survey, only weak earthquakes with magnitude $M_w < 5$ were recorded here [59]. Along the eastern side of the Darkhat Basin, the same-name fault zone divided into two segments by morphology stretches.

In the North Darkhat Fault zone, the Jaragol system of fault scarps with a height of 1.0–2.5 m and a minimum length of ~5 km was found [15, 37]. The recent morphotectonic and paleoseismic studies allowed to estimate the velocity of vertical (normal fault) displacements along the North Darkhat Fault at 0.3–0.6 mm/yr over the last ~8.4 ka, and to parameterize two paleoearthquakes with magnitudes $M_w = 7$ and an average period of recurrence of 3.5 ka [44]. The emplacement age of the Darkhat Basin (6.5–3.3 Ma) determined using the rates obtained is generally consistent with other data.

Khobsgol Basin. On the western wall of the Khobsgol Basin, triangular tectonic facets are clearly manifested along the West Khobsgol Fault zone. The facets are most fully developed in the northwestern part of the depression. In the southern direction the facets decrease in height; in the southernmost part of the basin the river valleys are incised into the upper level of the interbasin bridge, armored by Miocene basalts.

This is evidence of a decrease in tectonic activity in the southern direction. The normal fault activity at the northwestern segment is emphasized by a scarp, at the foot of which Late Holocene rockslides and ruptures at least 1000 years old were recorded. No distinct traces of later seismotectonic rupturing were found [15]. Apart from the well pronounced vertical component, remote sensing methods revealed dextral displacements of valleys along the Khobsgol fault zone by 30–50 and 100 m along NW-striking segments parallel to the lake shore [3]. Sinistral displacements of valleys and rock crests by up to 50 and 300–400 m, respectively, were detected along the NE-striking segments.

The Khubsugul earthquake with $M_w = 6.7$ and calculated intensity $I_o = 9$ MSK occurred in the northwestern part of the basin on January 12, 2021 [12]. During field seismotectonic studies using ESI-2007 scale, an epicentral zone with intensity $I_o = 8$ MSK was localized based on parameters of secondary disturbances [24].

At the condensation site of secondary disturbances, the earthquake source was found on the surface as a seismotectonic rupture oriented in the direction 340°–350° SSW and diagnosed as a dextral oblique fault with displacement by up to 20 cm in vertical and horizontal directions.

An earthquake epicenter was recorded in the Lake Khubsugul area at 18–19 km to the southeast from the earthquake source exposed on the surface [12]. The latter corresponds to the line with sharp change of interference pattern based on satellite radar interferometry data [29, 47, 56].

According to these data, the generalized model of the seismic fault represents the NW-striking plane (340°–350°) dipping in the eastern direction at angle of 45°–54° (i.e., toward the hypocenter). The fault plane reaches a depth of 18–24 km, with a vertical displacement at the surface of up to 20 cm. The short length of the traced rupture (~250 m) is apparently due to the small displacement magnitude, resulting in its preservation only in the central segment. Nevertheless, it was possible to identify a smoothed tectonic scarp with a height of ~1 m, formed due to previous movements and rejuvenated during the 2021 earthquake (Fig. 11).

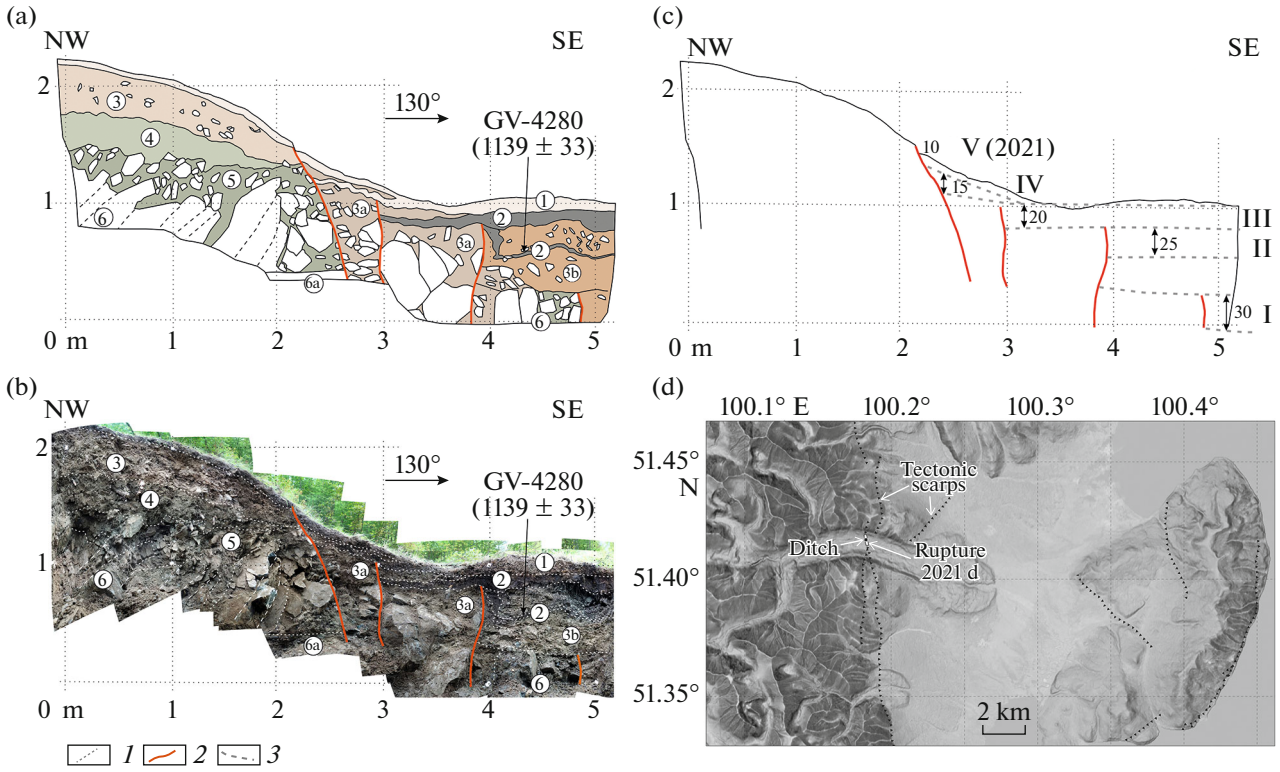

Fig. 11. Seismic rupture of 2021 Khubsugul earthquake. (a)–(b) northern wall of trench: (a) section, (b) panoramic photo; (c) reconstruction of succession of displacements; (d) location scheme of a seismotectonic rupture in Khubsugul earthquake source, a trench, and tectonic scarps. Circled numbers (a)–(b): (1) sod horizon of recent soil profile; (2) buried peaty horizons of paleosoils; (3) loose silt loams with rubble and grus (slope deposits), (3a) same, with boulders (colluvium), (3b) same, massive, lumpy, gleied; (4) grayish-green loams with rare rubble and gruss (finely-dispersed weathering crust); (5) rubble, boulders with sandy-loam matrix (clastic weathering crust); (6) ultramafic, highly fractured bedrocks, (6a) same rocks, weathered to clay state. (c) Cuccession of seismotectonic displacements (Roman numerals). (*1*) Fracturing in bedrock; (*2*) ruptures; (*3*) position of subsided fragments of Earth's paleosurface (displacement amplitudes are shown in centimeters in (c)).

In the trench section, the scarp clearly corresponds to a normal fault east-dipping at an angle of 50°–70°. At the edge of the scarp, the rupture displaces the modern soil surface by 10–15 cm. Ruptures of previous earthquakes, which successively involved all new areas on the side of the ridge in subsidence were revealed at the base of the scarp. In the section, such areas correspond to two buried peat horizons of paleosols (displacements by 25 and 20 cm) and a 15-cm sod horizon of recent soil split by a lens of slope material.

These horizons mark deformed fragments of the ancient earth surface. They are bounded by different-age faults and buried by slope material redeposited from the upthrown side. This indicates that the formation of each rupture was a one-act seismotectonic process. The younger rupture was emplaced to the west of the previous one, i.e., closer to the mountain massif. Thus, there was expansion of the basin with successive involvement of the adjacent part of the mountain uplift in the subsidence.

Among the samples taken for radiocarbon analysis, carbon date was obtained only for the lowest layer of peaty paleosol opened by the trench. Its calibrated age is 958–1176 years (radiocarbon date of 1139 ± 33 years, laboratory sample code is GV-4280) (see Fig. 11).

The humic acid date obtained is much younger, 836 ± 33 years. The paleosol dated with radiocarbon method was buried due to the displacement event (II). After this displacement (II), there were three more events: the displacement and burial of two paleosol horizons and the rejuvenation of the already existed rupture in 2021 (Fig. 11).

Consequently, four rupture-forming earthquakes have occurred over the last 958–1176 years with an average period of recurrence of 240–250 years. A total vertical displacement of 70 cm occurred at an average rate of 0.6–0.7 mm/yr over the last 958–1176 years. This estimate is slightly higher than the vertical displacement velocity along the North Darkhat Fault (0.3–0.6 mm/yr over the last ~8.4 ka [44]). This may be due to a shorter averaging time and/or increasing displacement rate with time.

The 2021 seismotectonic rupture is part of a system of tectonic scarps mapped in the foothills of the mountain massif in the northwest of the Khobsgol Basin. The scarps are of Late Holocene age. They disturb the surfaces of river terraces, moraines and glacial

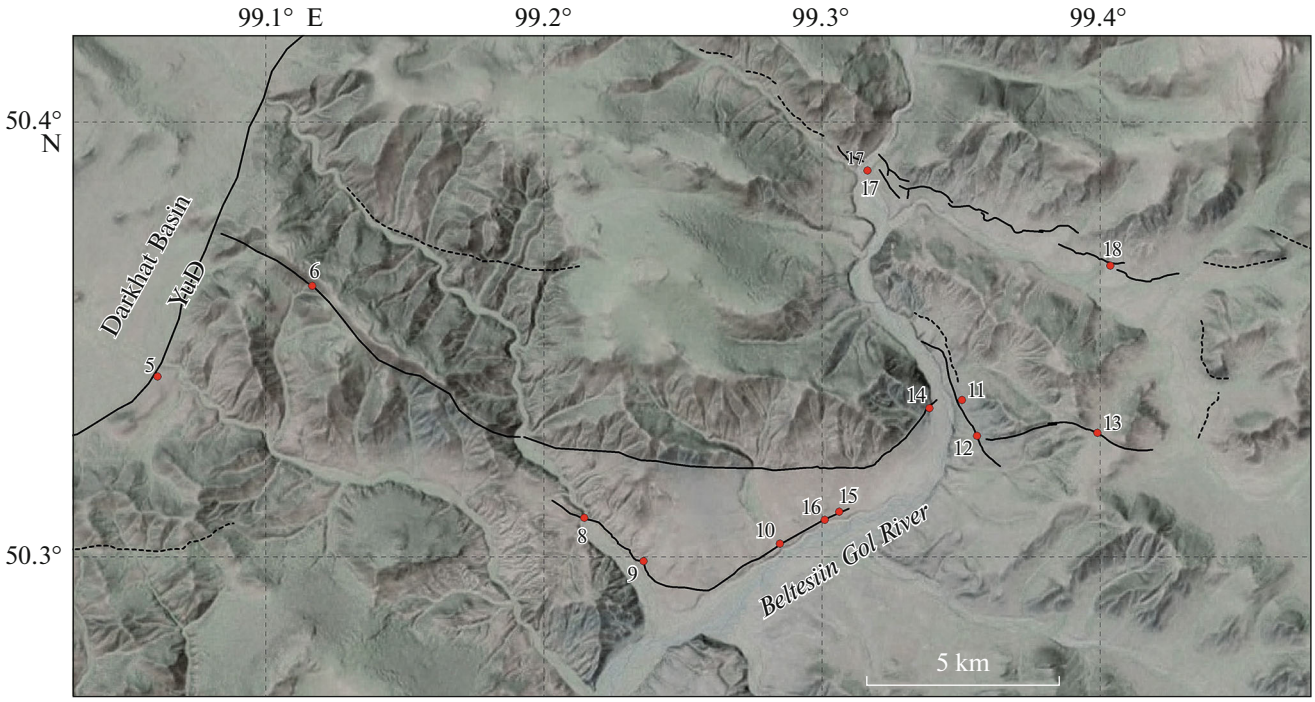

Fig. 12. Scheme of active faults between Darkhat Basin and Beltesiin Gol River valley. Faults with confirmed displacements of recent landforms are shown by solid lines; inferred faults based on remote sensing data are shown by dotted lines; sites with confirmed deformation of recent landforms are numbered in red (in circles).

troughs of the last large glaciation in the river valleys. Between river valleys the scarps are represented by a discontinuous chain of triangular tectonic facets. It is still unclear what segments of the fault zone identified in the trench, were affected by the previous ruptures. Accordingly, this makes it difficult to determine the magnitudes of paleoearthquakes.

Khobsgol–Darkhat interbasin bridge. In the northern part of the Khobsgol–Darkhat interbasin bridge, N.V. Lukina [18] interpreted the extended canyonlike erosional incision of the Maly Yenisei River with a tributary of the Kyzyl-Khem River as a manifestation of the active Kaakhem Fault (Kyzylkhem Fault, according to [51]). This fault is, a western, en echelon northward-displaced structural continuation of the Shishkhidgol Fault, which continues the Tunka–Mondy active fault zone with en echelon displacement to the south.

In the southern part of the Khobsgol–Darkhat interbasin bridge, the most striking manifestations of active tectonics are found east of the termination of the South Darkhat Fault, from which a fault zone with approximately W–E-trending, represented by several branches, branches off to the east. A tortuous tectonic scarp is traced along the main, most extended, branch, along the entire segment between the Darkhat Basin and the Beltesiin Gol River valley (Fig. 12).

In the bedrock section on the right wall of the Beltesiin Gol River valley, it is represented by an overthrust (dip angle 25°–30° in the NW direction) with a scarp on the surface of the 12-m high first above-flood-plain terrace (Figs. 13a, 13b).

It can be suggested that the height of the scarp directly reflects the magnitude of the vertical displacement along the fault, but the total displacement, given the gently dipping fault plane, is much greater. To the east of the Beltesiin Gol River, the scarp with the same sign dams up a small water catchment area, a marshy depression at the head of the stream (Figs. 13c, 13d). The strike of the scarp in this section is 300°–310° WNW.

The young age of displacement is confirmed by a rampart completely blocking the ruptured valley of a river, which has not had time to erode the tectonic dam and to incise a new channel since the last movement. In addition to the vertical component, a dextral shear component of displacement, by 36 m along the dry bed in the water catchment area, is observed.

To the south, an arcuate, very gentle, asymmetric rampart of up to 300 m wide with a steep southern slope was studied. The rampart separates the foothill base, a sloping plain, composed of young fluvial deposits, from the south. This plain is framing the foot of the mountain massif and is involved in a recent tectonic uplift. The structure of the southern, steep slope of the rampart was studied in a special clearing made in a temporary stream slope (Fig. 14).

A series of lenses/nappes, bounded by subhorizontal thrust faults, along which bedrock shales and diabases overthrust successively the variegated weathering crust, was uncovered at the base of the section.

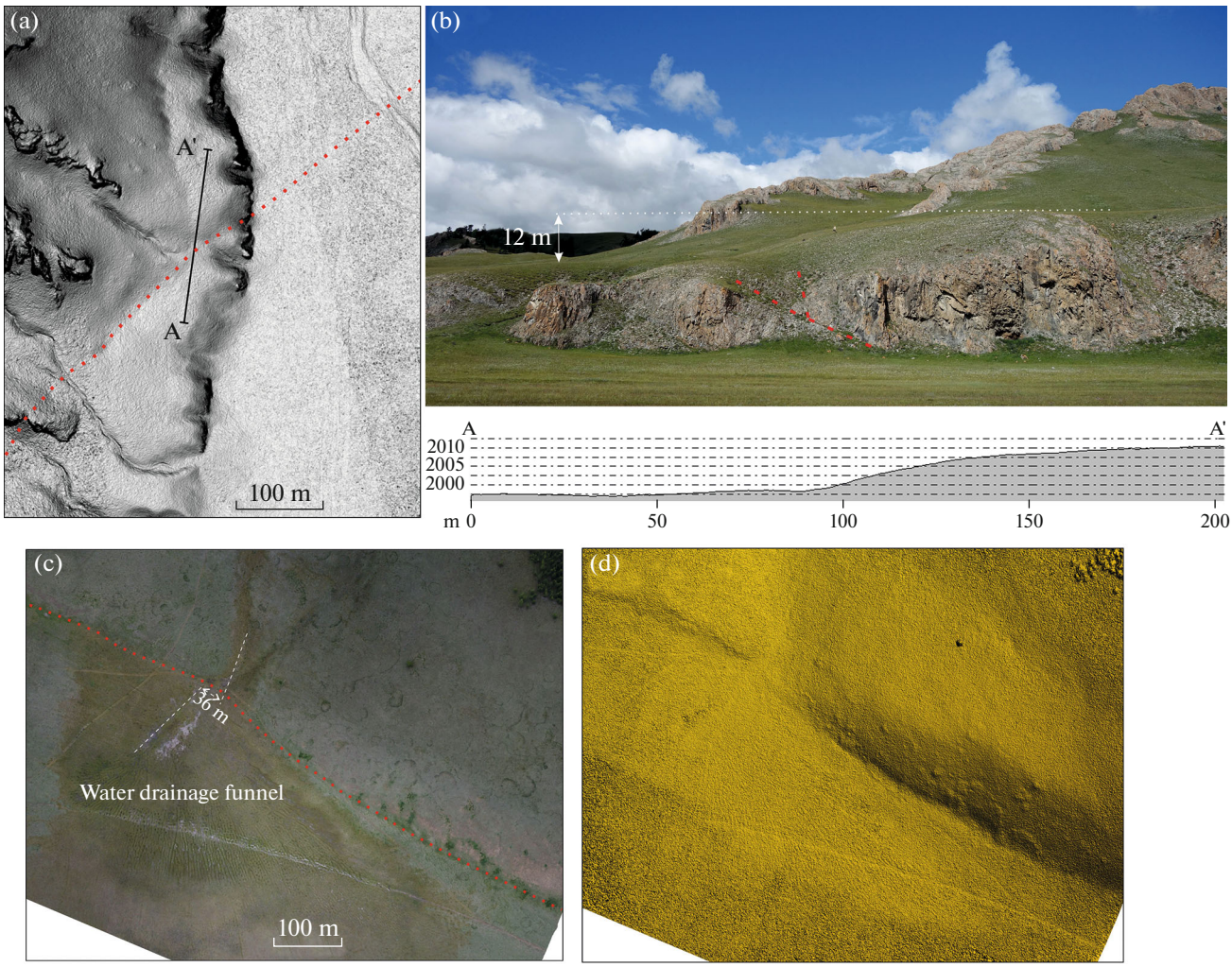

Fig. 13. Tectonic deformations of recent landforms in Beltesiin Gol River valley and its environs. Active faults are shown by dashed lines. (a)–(b) Right side of Beltesiin Gol River valley (point 14 in Fig. 12): (a) digital elevation model based on aerial photography data; (b) a general view (photo) and profile of scarp based on results of ground measurements and on digital elevation model; (c)–(d) tectonic dam and dextral strike slip of a dry channel (p. 13 in Fig. 12): (c) aerial photograph from drone, (d) digital elevation model.

Younger slope deposits were also involved in later thrusting. It is important to note the bending of the alluvial–proluvial strata (2), conformal to the thrust-related anticlinal fold in the diabases, which making up the hanging wall of the thrust, and the bending of the surface of the first above-flood-plain terrace (Fig. 14). One can assume that the arcuate rampart was formed due to thrust-related bending of young deposits.

RELATIONSHIP OF ACTIVE FAULTS, NEOTECTONIC STRUCTURE, AND DEEP STRUCTURE OF THE STUDY AREA

System of Active Faults as a Structural Paragenesis

The considered region is bounded by two W–E-trending sinistral strike-slip zones: the Khangai in the south and the Tunka–Mondy in the north. The Erzin–Agardag and Tsetserleg sinistral oblique-slip faults are auxiliary to the Khangai Fault in the north and extend north-northeast. En echelon series of the Busiyngol, Darkhat, and Khobsgol grabens are located at the east-northeast extension of the Erzin–Agardag Fault, which in the northeast is attached to the southern end of the Busiyngol graben, the western member of the series.

The northern end of the Khobsgol graben, the eastern member of the en echelon series, meets with the western end of the Tunka–Mondy zone. The normal faults, which bound the Khobsgol graben in the west, are traced southward almost to the Tsetserleg Fault zone. To the east of their convergence zone, manifestations of the Tsetserleg Fault activity become less pronounced; at ~100 km, traces of fault activity disappear.

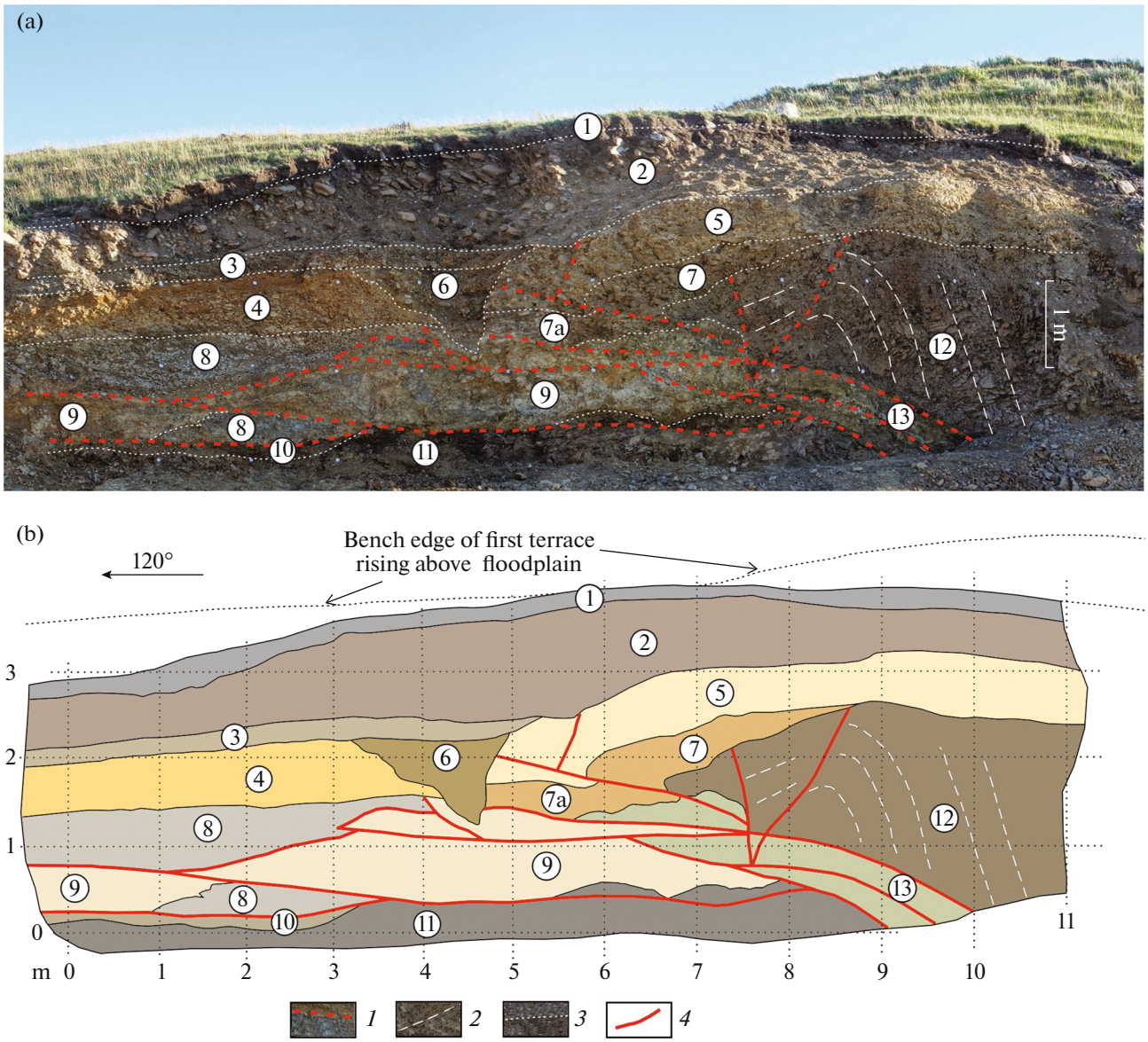

Fig. 14. Photo (a) and sketch (b) of thrust fault in right side of Beltesiin Gol River valley at site 10 where neotectonic deformation landforms were confirmed. For position of site 10, see Fig. 12. Arabic numerals in circles: (1) humus horizon of modern soil profile; (2) semi-rounded pebbles, boulders with sandy-gravel matrix (proluvial-alluvial deposits); (3) layered debris, rare boulders, sometimes semi-rounded, with brownish-gray sandy loam matrix (proluvial–slope deposits); (4) layered debris (mostly shales) with brown sandy loamy matrix (slope deposits); (5) flattened rubble, less frequently blocks of various rocks with brownish-brown loamy matrix (slope deposits); (6) pebbles, rubble with loamy-sandy-gravelstone matrix (proluvial–colluvial deposits, filling erosional incision or extension fracture); (7) rubble, blocks of bedrock diabase (redeposited detrital weathering crust), (7a) same, with sandy loam matrix; (8) weathered, strongly fractured clayey shales, which lie as large fragments in variegated loams; (9) variegated (brown, with gray spots) lumpy loams with rubble and rare blocks of various rocks (weathering crust); (10) rubble, gruss (weathered, strongly fractured clay shales); (11) dark gray clay shales, brecciated, mylonitized; (12) strongly fractured, crushed diabase; (13) dark-green clay gouge with rubble and grus of bedrocks. *1*, ruptures (a); *2*, fracturing along foliation in diabases; *3*, stratigraphic contacts; *4*, ruptures (b).

Thus, the active faults of the region form an interconnected system.

Active thrusts, reverse faults and small fault-related folds of sedimentary strata of W–E and northwestern strike are associated with N–S-trending faults of en echelon series of grabens in the south. They are found between the southern ends of the Darkhat and Khobsgol graben troughs at the eastern end of the Erzin-Agardag Fault.

Such a combination of normal faults as manifestations of extension with thrusts, reverse faults, and fault-related folds as manifestations of horizontal compression is characteristic of strike-slip deformation zones. In this case, they form a sinistral zone of deformation

located between the ends of two sinistral strike-slip faults, the Erzin–Agardag Fault and the Tunka–Mondy zone, which plays the same kinematic role.

To understand the geodynamic conditions of the development of the structural paragenesis described above, it is important to elucidate the origin of the Khangai and Tunka–Mondy W–E-trending sinistral strike-slip zones.

P. Freund [53] divided the strike-slip faults into transform and transcurrent ones. Paying attention to the kinematic features, we distinguished displacement and rotational strike-slip faults, which are similar in characteristics to the transform and transcurrent faults of Freund [53], respectively, and supplemented these two types with squeeze strike-slip faults, which are formed when rocks lying between two fault zones are squeezed towards less horizontal compression [31].

The displacement strike-slip fault is characterized by sustained strike and displacement amplitude and the presence of compensating compression or extension structures at the ends of the fault. It develops at a large radius of rotation of sides of the fault with the center extending beyond the limits of the faulted tectonic area, within of which is understood as the result of translational displacement of one side relative to the other.

Displacements along a rotational strike-slip fault are less sustained and attenuate toward its terminations. A shear develops when there is a rotational component in rock movement, with the center of rotation close to the fault. The study of natural strike-slip faults shows that the features of the above types are often combined.

The Khangai and Tunka-Mondy sinistral fault zones are parts of a more extensive system of paragenetically related active faults of Mongolia and Southern Siberia. Therefore, they can be considered as displacement strike-slip faults [33]. This system is characterized by the orientation of relative horizontal compression from southwest to northeast and extension from northwest to southeast, with compression dominating in the west and center of Mongolia and adjacent parts of Southern Siberia and extension in the northeast of the region, in the Baikal Rift Zone, and in Transbaikalia.

At the same time, the structure of the Khangai Fault zone has signs of rotational shear. They are manifested in the fact that in the east the fault zone degenerates without transferring the strike-slip amplitude to compensating structures. In the west, the strike-slip amplitude decreases and the zone divides into several branches with no direct connection with faults of Mongolian Altai. This suggests that under transverse compression, strike-slip movements along the Khangai and Tunka–Mondy fault zones were partially caused by clockwise rotation of the block located between them.

The rotation of the interfault block changed the position of the principal axes of normal stress in it. Relative compression became N–S-trending, and extension, W–E-trending, manifested in the east-northeast strike of the Erzin–Agardag and Tsetserleg Strike-slip faults and the N–S orientation of the grabens of en echelon series.

Comparison of Active Faults with Neotectonic Elements

The considered region encompasses two major elements of the neotectonic structure: the Khangai dome-shaped uplift and the western and northern parts of the C-shaped belt of intermontane basins flanking the uplift. The investigated part of the C-shaped belt includes Tunka Basin in the north, Ubsu-Nur Basin in the west, and the Khan-Khuhiin Ridge between this basin and the Great Lakes Depression located southward. The southern part of the Khangai dome-shaped uplift, uplifted to 4000 m, is higher than its northern part, uplifted to 3000 m, and is separated from the latter by a smooth tectonic scarp up to 500–700 m high [33].

The northern part connects with the mountain structures of East Tyva in the north. No major recent faults have been detected at the boundary between the Khangai uplift and the belt of depressions. They are present at the outer boundaries of the belt of basins: the Tunka Basin at the boundary to the East Sayan and Tunkinskie Goltsy, Great Lakes Depression, and Valley of Lakes at the boundaries to Mongolian and Gobi Altai.

The time of onset of the formation of the neotectonic structure in the region can be considered Late Oligocene, when depressions of the C-shaped belt were appeared around the Khangai uplift, although the latter itself began to rise earlier [33]. The contrast between the vertical movements of the Khangai dome-shaped uplift and the neighboring basins increased with time.

The structural pattern formed by the above elements of the neotectonic structure and their fault constraints differs from that formed by active faults. At the same time, some large active faults partially inherit elements of the neotectonic structural pattern. This is primarily related to faults of the eastern front of Mongolian Altai [9]. The geological evolution of the Khangai Fault is less certain. Its western part extends along the northern slope of the uplift of the Khan-Khuhiin Ridge, which was appeared no later than the Pliocene, while the eastern part of the fault follows the tectonic scarp separating the more uplifted southern part of the Khangai dome-shaped uplift from its northern part.

In both parts of the fault, the vertical component of Late Quaternary movements coincides with that of earlier movements. During the Late Quaternary stage, the vertical component is many times inferior to the strike-slip component of movements. There are no grounds to assume similarly significant lateral movements at earlier stages of development. The Tunka–

Mondy zone of active faults inherits the fault zone, which bounds a chain of the Tunka basins in the north. However, the direction of vertical movements along active faults is opposite to the movements at the boundaries of basins during sedimentation [43]. The extent of strike-slip movements in that epoch is unclear.

Active faults between the Khangai and Tunka–Mondy strike-slip zones (Erzin–Agardag and Tsetserleg faults, grabens of en echelon series) are discordant with respect to the elements of the neotectonic structure and appear to complicate it. The relative subsidence of the southern wall of the Tsetserleg active fault is consistent with the subsidence of the surface of the Khangai dome-shaped uplift between the Khangai and Tsetserleg faults. The flat Muren Basin confined to this depression is filled with Upper Pliocene–Quaternary deposits up to 100 m thick [15]. Deposits of different stages of Pleistocene and probable analogs of the Upper Pliocene Ocherous Formation of the Tunka Basin were uncovered on the sides of the Darkhat and Khobsgol troughs. Apparently, the graben-shaped basins of the Cis-Khobsgol region appeared in the Pliocene.

Thus, in addition to signs of inheritance of active faults, there are signs of structural rearrangement of the early elements of the neotectonic structure that led to the formation of the recent network of active faults in the region. The first signs of transformations associated with the paragenesis of active faults date back to the Late Pliocene. The subsidence of the Tunka Depression and, consequently, subsidence of the southern flank of the Tunka–Mondy zone lasted until the Early Pleistocene and ended not earlier than the basaltic volcanism with an age of ~1.6 Ma in the upper half of the sandy formation crowning the section of the depression [25, 65].

Consequently, changes in the direction of vertical movements in this zone occurred later; i.e., rearrangement of the neotectonic structure that led to the final formation of the active fault system was completed not earlier than the end of the Early Pleistocene. This does not exclude the fact that the elements of the structural paragenesis of active faults, and the paragenesis represented by the Khangai dome-shaped uplift and the framing belt of basins, could have developed simultaneously, being associated with different geodynamic sources [33].

Comparison of Active Faults with the Structure of the Earth's Crust and Upper Mantle

The crustal thickness of the considered region was estimated from gravity data [13–15]. According to calculations, the crustal thickness under the Siberian Platform is estimated at 39–43 km. It increases to 44–45 km beneath the Great Lakes Basin and 46–52 km under East Sayan and Cis-Khobsgol, decreasing by 5–6 km beneath the Darkhat and Khobsgol grabens and reaching 60 km beneath Southern Khangai and Mongolian Altai.

Interpretation of the gravity data revealed the existence of large volumes of abnormal (decompressed) mantle beneath Mongolia and Transbaikalia, the roof of which can rise to depths of 40–50 km, partially or completely replacing the mantle part of the lithosphere and reaching the crustal basement in some places [13, 14].

The use of the MITP08 seismotomographic model [55], which shows the deviation of *P*-wave velocities from the average values for the corresponding depths, made it possible to refine the distribution of different velocity volumes in the upper mantle and identify and delineate the complex Khangai plume ascending from a depth of ~1300 km [33].

We present a structural map of the roof of the Khangai plume along the $\delta V_p = -0.5\%$ isosurface, based on the MITP08 velocity model (Fig. 15).

Above the main body of the plume, the roof of the low-velocity mantle rises to depths less than 67 km. This rise of the low-velocity mantle extends from the Beishan Mountains to the north, encompassing the ridges of the Eastern Tien Shan, Gobi Altai, the Valley of Lakes, the Great Lakes Depression, and the Southern Khangai uplift, to the Khangai Fault.

Northward, there is a smaller area of uplifting of low-velocity mantle, falling within the Darkhat and Khubsugul graben troughs and their mountain frames. It is separated from the main uplift by the Muren bridge bounded by the Tsetserleg Fault and the eastern part of the Khangai Fault. Under the bridge, the roof of the low-velocity mantle is located at a depth of at least 100 km.

Rises of the top of the low-velocity mantle (decompacted and, probably, abnormally overheated) are surrounded by areas where the mantle top descends. This is especially sharp and contrasting to a depth of about 250 km, in the northern part of the region at the boundaries with Mongolian Altai, the Ubsu-Nur Basin, the mountain structures of East Tyva, East Sayan, and Khamar-Daban, and the eastern slope of the Khangai dome-shaped uplift. Beneath the Siberian Platform, the high-velocity mantle is traced from the crustal basement to a depth of 1100 km and there are no signs of a plume.

All major active strike-slip zones are either located in the areas of lowered top of the mantle plume or, more often, at the boundaries of plume protrusions, where its top descends. Thus, strike- and oblique-slip faults in Mongolian Altai extend along the western boundary of the main low-velocity mantle protrusion.

The Khangai Fault in the western part is located at the northern boundary of the main protrusion, while in the eastern part, it forms the southern boundary of the junction between the main protrusion of the low-

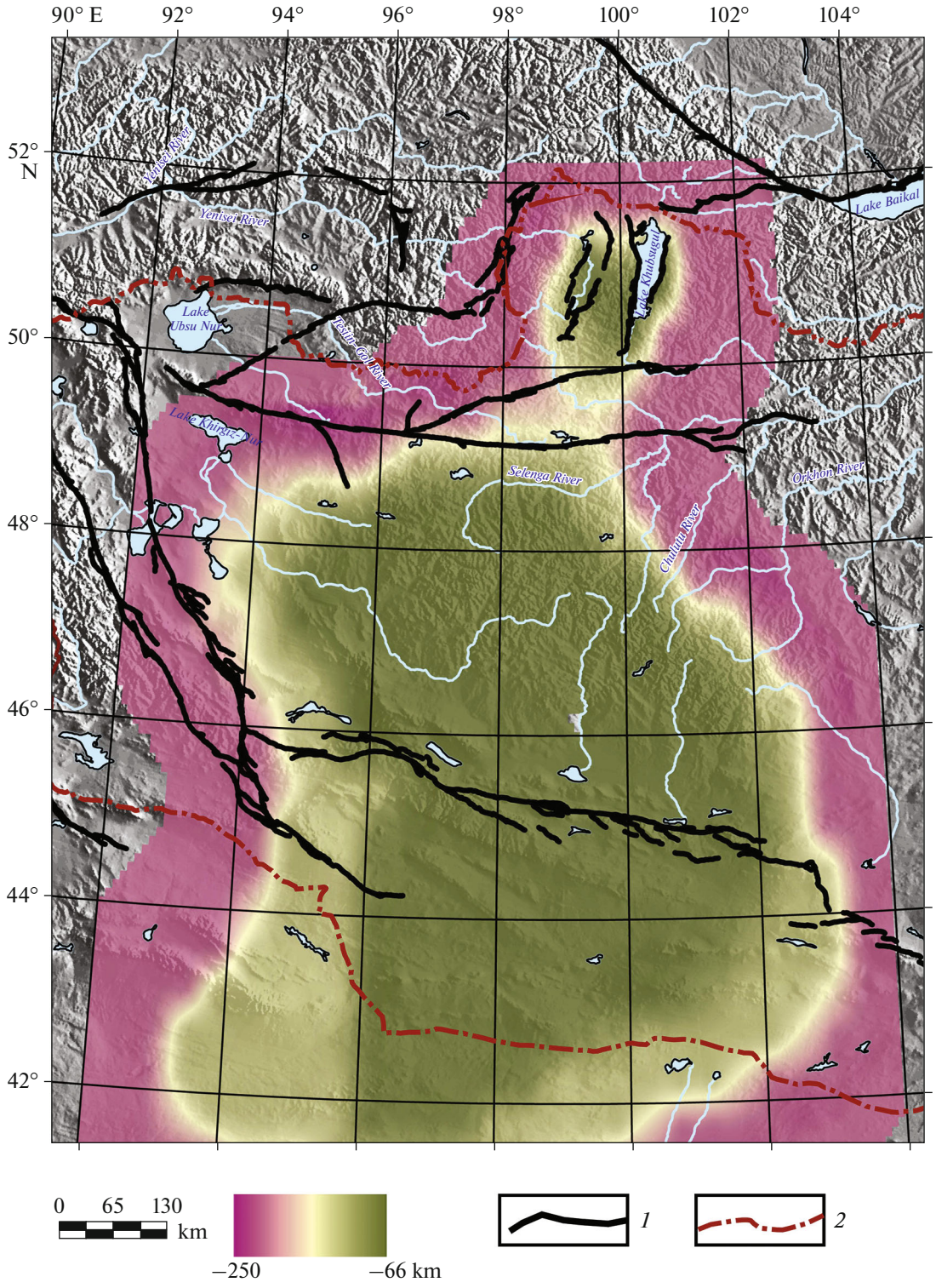

Fig. 15. Comparison of active faults of Western and Central Mongolia and adjacent part of Southern Siberia with position of top of low-velocity mantle on $\delta V_p = -0.5\%$ isosurface (based on MITP08 velocity model [55]). (*1*) active faults; (*2*) state border.

velocity mantle and the small protrusion of Cis-Khubsugul. The Tsetserleg strike-slip fault forms the northern boundary of this bridge. The Erzin–Agardag oblique-slip fault and Tunka-Mondy strike-slip zone are located in areas where the top of the mantle plume descends. In contrast, the Darkhat and Khobsgol grabenlike depressions are located within a small low-velocity mantle protrusion.

DISCUSSION

Comparison of active faults with the position of the top of the low-velocity mantle on the $\delta V_p = -0.5\%$ isosurface shows that all faults with a dominant strike-slip component of displacement are located in parts of the region where the top of the low-velocity mantle has subsided to the extent that a significant portion of the lithospheric mantle is preserved above it. In stating this, we realize that the $\delta V_p = -0.5\%$ isosurface constrains the mantle region with obviously lower *P*-wave velocities, where the strength of rocks is reduced. Above this surface, there may be volumes of mantle rocks, also decompacted, with less reduced *P*-wave velocities.

In areas where the –0.5% isosurface is not deeper than 67 km, the mantle part of the lithosphere is significantly reduced or absent, and the Earth's crust is exposed to the anomalous mantle. Probably, due to this, the Erzin–Agardag strike-slip fault and Tunka–Mondy strike-slip zone are replaced above the low-velocity mantle protrusion between them by the zone of strike-slip deformation, which is represented by a number of grabens. Significant extension of the crust of the grabens, comparable to the strike-slip magnitude, is indicated by a 5–6-km decrease in crustal thickness beneath the grabens [15].

The epicenters and focal zones of the strongest earthquakes, the Bolnai ($M_w \geq 8$) and Tsetserleg ($M_w = 8$), in the considered region covered different elements of the neotectonic structure. Thus, the epicenter of the Bolnai earthquake was located in the Khan Huhiy Ridge between the Great Lakes Depression and the Ursu-Nur Basin, i.e., within the C-shaped belt of basins, and the focal zone of not less than 375 km in length, marked by seismic ruptures along the Khangai Fault and conjugated faults spreading from the epicenter both to the west and east, towards the Khangai dome-shapes uplift.

The epicenter of the Tsetserleg earthquake and its 190 km-long focal zone are located in the northern part of the Khangai dome. Given such large sizes of the focal zones of both earthquakes, it is reasonable to assume that they were not limited to the seismogenic upper crustal layer, but also encompassed deeper layers of the lithosphere up to its mantle part.

It is shown that focal zones of both earthquakes are located in areas where the top of low-velocity mantle descends and allows preservation (at least partial) of mantle part of lithosphere, which is quite consistent with propagation of the focal zone up to these depths (Fig. 15).

In contrast to these strongest earthquakes, the origin of the Khubsugul earthquake ($M_w = 6.7$) on January 12, 2021 is located above the low-velocity mantle protrusion, where the mantle part of the lithosphere is extremely reduced or absent. This constrains the depth of the source area to the upper crustal layer, which is consistent with the source area at a depth of 18–24 km calculated by comparing seismic ruptures exposed on the Earth's surface, the inclination of a seismogenic fault, and the position of the earthquake epicenter [29, 47, 56].

The presented ideas about dependence of lateral sizes of the earthquake focal zone and magnitude on the depth, to which the focal zone extends, contradict the data on the Gobi–Altai earthquake (1957), which activated the 180-km Dolinoozersky segment (Bogd Fault) of the Gobi–Altai active sinistral oblique-slip fault zone. The amplitude of earthquake-triggered strike-slip fault was 5 m, locally up to 8 m [7, 19, 32]. The magnitude of the earthquake was $M_s = 8$.

The focal zone of the earthquake, marked by seismic ruptures, is entirely located above the low-velocity mantle protrusion of the Khangai plume, where the mantle part of the lithosphere is highly reduced or absent, and the lower part of the crust could have softened under the effect of the plume. Thus, the focal zone did not extend beyond the upper crustal seismogenic layer.

It is possible to explain the occurrence of the strongest earthquake with a shallow focal area by assuming temporal heterogeneity of the stress field with a periodic or aperiodic increase om stress, at which large volumes of the crust in active zones can be subjected to simultaneous destruction.

The possibility of such an increase in stress with simultaneous reorientation of the stress axes was demonstrated with examples of the El Gab northern segment of the Dead Sea Transform and Talas–Fergana faults [66]. Probably, the Gobi-Altai seismic event is similar to the East Anatolian earthquake on February 6, 2023, with $M_w = 7.8$, the focal zone of which spread, as evidenced from the appeared seismic ruptures to 361 km along the East Anatolian sinistral fault zone with a hypocentral depth of ~10 km [39].

CONCLUSIONS

The active tectonics of northern Central Mongolia and the adjacent part of Southern Siberia is governed by movements along two W–E-trending sinistral strike-slip zones: the Khangai Fault and the Tunka–Mondy zone. The strike-slip rate along the Khangai Fault is a few mm per year; along the Tunka–Mondy zone—1.1–1.5 mm/yr. These faults are part of a uniform ensemble of the largest active faults in the Mongolia–Baikal region, formed under conditions of northeastern maximum compression and northwestern maximum extension.

The E–NE-striking Erzin–Agardag and Tsetserleg faults, with a dominant sinistral strike-slip component of displacements are auxiliary to the Khangai Fault and stretch between these two fault zones. Between the eastern end of the Erzin–Agardag strike-slip zone and the western part of the Tunka–Mondy strike-slip

zone, there is a series of N–S-trending asymmetric grabenlike troughs (Busiyngol, Darkhat, and Khobsgol). This series forms a sinistral zone of strike-slip deformation that plays the same kinematic role as the faults at the continuation of the series.

The faults that developed between the Khangai Fault and Tunka–Mondy zone form a structural paragenesis, which differs in geodynamic parameters from those of the main boundary faults and evidence its formation under conditions of N–S-trending relative compression and W–E-trending extension. The change in orientation of the axes of the main normal stresses may be due to clockwise rotation of the block between the boundary faults.

In the mantle, beneath the considered area, there is a volume of reduced seismic wave velocities, which we consider the Khangai plume. The decrease in velocity may reflect heating and decompaction of mantle rocks. The top of the significantly decompacted mantle above the axial part of the plume is located above a depth of 67 km, which reflects thinning (in some places up to complete disappearance) of the lithospheric mantle and may be responsible for the decompaction of its preserved part. Active strike-slip faults in the region developed along the periphery of the low-velocity mantle uplift, where the thickness of the strong lithosphere increases. In the axial part of the uplift, strike-slip faults are replaced by a zone of strike-slip deformation represented by grabenlike depressions. As our trenching has shown, the recurrence of strong earthquakes was more frequent here than in the strike-slip zones, but they were characterized by smaller magnitudes.

ACKNOWLEDGMENTS

The authors would like to thank E.V. Parkhomchuk (Center for Collective Use "Accelerator Mass Spectrometry of NSU-NSC," Novosibirsk, Russia) for preparation of radiocarbon samples and their radiocarbon dating and E.A. Zelenin (Geological Institute, Russian Academy of Sciences, Moscow, Russia) for assistance in calibrating radiocarbon dates obtained for the Khangai Fault zone. The authors thank the reviewer A.F. Emanov (Altai-Sayan Branch, Federal Research Center Geophysical Service, Russian Academy of Sciences, Novosibirsk, Russia), the anonymous reviewer for helpful comments, and editor M.N. Shoupletsova (Geological Institute, Russian Academy of Sciences, Moscow, Russia) for careful editing.

FUNDING

The relations of active faults with the neotectonic structure of the region were studied within the budget framework FMMG-2023-0006 of the Geological Institute, Russian Academy of Sciences. The rest of the research and preparation of the paper were supported by the Russian Science Foundation, project no. 22-17-00049.

CONFLICT OF INTEREST

The authors of this work declare that they have no conflicts of interest.

REFERENCES

1. S. G. Arzhannikov and A. V. Arzhannikova, "The paleoseismogenic activation of the Great Lakes segment of the Erzin–Agardag fault," Volcanol. Seismol., No. 2, 56–66 (2009).
2. A. V. Arzhannikova, *Doctoral Dissertation in Geology and Mineralogy* (Inst. Zemn. Kory Sib. Otd. Ross. Akad. Nauk, Irkutsk, 2021).
3. A. V. Arzhannikova, A. V. Parfeevets, V. A. San'kov, and A. I. Miroshnichenko, "Late Cenozoic kinematics of active faults in the Hovsgol basin (southwestern flank of the Baikal Rift)," Russ. Geol. Geophys. **44** (11), 1162–1167 (2003).
4. A. V. Arzhannikova, V. I. Mel'nikova, and N. A. Radziminovich, "Late Quaternary and current deformation in the western Tunka system of basins: evidence from structural geomorphology and seismology," Russ. Geol. Geophys. **48** (4), 305–341 (2007).
5. V. V. Vdovin, "Traces of earthquakes in the Belino-Busingol depression of Eastern Tuva," in *Seismogeology of the Eastern Altai-Sayan Mountain Region*, Ed. by V. P. Solonenko (Nauka, Novosibirsk, 1978), pp. 68–72.
6. A. V. Voznesensky, "The study of the Khangai farming area in 1905 in Northern Mongolia," in *Materials for the Department of Physical Geography,* Vol. 1 (RGO SSSR, Leningrad, 1962). 51 p. [in Russian].
7. *Gobi–Altai Earthquake*, Ed. by N. A. Florensov and V. P. Solonenko (Akad. Nauk SSSR, Moscow, 1963) [in Russian].
8. E. V. Devyatkin, The Cenozoic of Inner Asia: Stratigraphy, geochronology, and correlation, in *Transactions of Joint Soviet-Mongolian Geological Expedition* (1981). Vol. 27, Ed. by K. V. Nikiforova (Nauka, Moscow, 1981) [in Russian].
9. E. V. Devyatkin, "Inner Asia," in *Neotectonics, Geodynamics, and Seismicity of Northern Eurasia*, Ed. by A. F. Grachev (Inst. Fiz. Zemli Ross. Akad. Nauk, Moscow, 2000), pp. 92–100.
10. E. V. Devyatkin, E. M. Malaeva, V. S. Zazhigin, V. E. Murzaeva, N. A. Korina, N. B. Glukhovskaya, T. Semeikhan, I. P. Syrnev, T. V. Nikolaeva, Yu. L. Ivanov, A. F. Boishenko, T. V. Lopatin, G. A. Shmidt, N. I. Shveiskii, N. G. Ivanova, V. A. Kulakov, V. A. Belova, and G. N. Shilova, "Late Cenozoic of Mongolia (stratigraphy and paleogeography)", in *Transactions of Joint Soviet-Mongolian Geological Expedition.* Vol. 47, Ed. by N. A. Logachev (Nauka, Moscow, 1989) [in Russian].
11. A. F. Emanov, A. A. Emanov, A. V. Fateev, V. M. Solov'ev, E. V. Shevkunova, E. A. Gladyshev, I. A. Antonov, D. G. Korabel'shchikov, V. G. Podkorytova, V. V. Yankaitis, S. A. Elagin, N. A. Serezhnikov, A. V. Durachenko, and A. I. Artemova, "Seismological studies in the Altai–Sayan mountain region," Russ. J. Seismol. **3** (2), 20–51 (2021). https://doi.org/10.35540/2686-7907.2021.2.02

12. A. F. Emanov, A. A. Emanov, V. V. Chechel'nitskii, E. V. Shevkunova, Ya. B. Radziminovich, A. V. Fateev, E. A. Kobeleva, E. A. Gladyshev, V. V. Arapov, A. I. Artemova, and V. G. Podkorytova, "The Khuvsgul earthquake of January 12, 2021 (M_W = 6.7, M_L = 6.9) and early aftershocks," Izv., Phys. Solid Earth **58** (1), 59–73 (2022). https://doi.org/10.31857/S0002333722010021
13. Yu. A. Zorin, V. V. Mordvinova, M. R. Novoselova, and E. Kh. Turutanov, "Density heterogeneity of the mantle under the Baikal Rift," Izv. Akad. Nauk SSSR. Ser. Fiz. Zemli, No. 5, 43–52 (1986).
14. Yu. A. Zorin, M. R. Novoselova, and V. A. Rogozhina, *Deep Structure of Mongolia*, Ed. by N. A. Logachev (Nauka, Novosibirsk, 1982) [in Russian].
15. V. M. Kochetkov, S. D. Khil'ko, Yu. A. Zorin, et al., *Seismotectonics and Seismicity* of the Cis-Khubsugul Area, Ed. by N. A. Logachev (Nauka, Novosibirsk, 1993) [in Russian].
16. N. A. Logachev, "Historic core of the Baikal Rift Zone," Dokl. Earth Sci. **376** (4), 43–46 (2001).
17. N. A. Logachev, I. V. Antoshchenko-Olenev, D. B. Bazarov, V. I. Galkin, G. S. Goldyrev, A. S. Endrikhinskii, A. G. Zolotarev, A. I. Sizikov, and G. F. Ufimtsev, *The Development History of the Topography of Siberia and the Far East. The Highlands of the Baikal Region and Transbaikalia*, Ed. by N. A. Florensov (Nauka, Moscow, 1974) [in Russian].
18. N. V. Lukina, "Altai–Sayan area of recent ridging of continental lithosphere. Baikal intracontinental rift system," in *Neotectonics and Recent Geodynamics of Mobile Belts*, Ed. by P. N. Kropotkin (Nauka, Moscow, 1988), pp. 276–326 [in Russian].
19. A. V. Lukyanov, "Horizontal movements along faults during modern catastrophic earthquakes," in *Faults and Horizontal Movements of the Earth's Crust*, Ed. by A. V. Peive (Akad. Nauk SSSR, Moscow, 1963), pp. 34–112 [in Russian].
20. V. N. Mazilov, S. A. Kashik, and T. K. Lomonosova, "Oligocene deposits in the Tunka trough (Baikal rift zone)," Geol. Geofiz. **34** (8), 81–88 (1993).
21. V. D. Mats, G. F. Ufimtsev, M. M. Mandel'baum, A. M. Alekshin, A. V. Pospeev, M. N. Shimaraev, and O. M. Khrustov, *Cenozoic of the Baikal Rift Trough: Structure and Geological History* (GEO, Novosibirsk, 2001) [in Russian].
22. A. A. Mossakovsky, S. V. Ruzhentsev, S. G. Samygin, and T. N. Kheraskova, "Central Asian Fold Belt: Geodynamic evolution and history of formation," Geotektonika, No. 6, 3–32 (1993).
23. *New Catalog of Earthquakes in the USSR Territory from Ancient Times to 1975*, Ed. by N. V. Kondorskaya and N. V. Shebalina (Nauka, Moscow, 1977) [in Russian].
24. A. N. Ovsyuchenko, S. Demberel, Yu. V. Butanaev, N. G. Koshevoi, Ts. Batsaikhan, and N. Baatar, "The Khubsugul earthquake of January 12, 2021, M_w = 6.7, Northern Mongolia: Geological effects and tectonic position of the source," Dokl. Earth Sci. **511** (1), 566–570 (2023). https://doi.org/10.31857/S2686739723600455
25. S. V. Rasskazov, V. A. San'kov, V. V. Ruzhich, and O. P. Smekalin, *Cenozoic Continental Rifting: Guide of Geological Excursions in Tunka Rift Basin* (Inst. Zemn. Kory Sib. Otd. Ross. Akad. Nauk, Irkutsk, 2010) [in Russian].
26. O. P. Smekalin, *Study of Paleoseismogenic Deformations of the Southern Baikal Region*, Ed. by E. A. Rogozhin and V. S. Imaev (Inst. Fiz. Zemli Ross. Akad. Nauk, Moscow, 2008) [in Russian].
27. S. A. Sokolov, S. T. Garipova, K. I. Yushin, Yu. V. Butanaev, E. A. Zelenin, A. N. Ovsyuchenko, and S. V. Maznev, "The neotectonic structure of the northern framing of the Ubsunur Depression and its relation with active faults (Republic of Tuva, Russia)," Geotectonics **57** (1), 82–99 (2023).
28. A. M. Sugorakova, V. V. Yarmolyuk, and V. I. Lebedev, *Cenozoic Volcanism of Tuva*, Ed. by A. E. Izokh (Tuv-IKOPR SO RAN, Kyzyl, 2003) [in Russian].
29. E. P. Timoshkina, V. O. Mikhailov, V. B. Smirnov, M. S. Volkova, and S. A. Khairetdinov, "Model of the rupture surface of the Khuvsgul Earthquake of January 12, 2021 from InSAR data," Izv., Phys. Solid Earth **58**, 74–79 (2022).
30. V. G. Trifonov, "Features of the development of active faults," Geotectonics, No. 2, 16–26 (1985).
31. V. G. Trifonov, E. A. Zelenin, S. Yu. Sokolov, and D. M. Bachmanov, "Active tectonics of Central Asia," Geotectonics **55**, 361–376 (2021).
32. V. G. Trifonov and V. I. Makarov, "Active faults (Mongolia)," in *Neotectonics and Recent Geodynamics of Mobile Belts* (Nauka, Moscow, 1988), pp. 239–272 [in Russian].
33. V. G. Trifonov, S. Yu. Sokolov, S. A. Sokolov, S. V. Maznev, K. I. Yushin, and S. Demberel, "Khangai intramantle plume (Mongolia): 3D model, influence on Cenozoic tectonics, and comparative analysis," Geotectonics **57** (6), 774–806 (2023). EDN: GFPLXF https://doi.org/10.31857/S0016853X23060073
34. A. P. Fedotov, *Doctoral Dissertation in Geology and Mineralogy* (Kazan. Gos. Univ., Kazan, 2007).
35. D. R. Hutchinson, A. Yu. Golmshtok, L. P. Zonenshain, T. C. Moore, C. A. Scholz, and K. D. Klitgord, "Structural features of the sedimentary sequence of Lake Baikal based on the multichannel seismic survey data," Geol. Geofiz. **34** (10–11), 25–36 (1993).
36. S. D. Khil'ko and M. Balzhinnyam, "Morphostructure and seismotectonics of Northern Mongolia," in *Seismotectonics of the Southern USSR*, Ed. by I. E. Gubin (Nauka, Moscow, 1978) [in Russian].
37. S. D. Khil'ko, R. A. Kurushin, V. M. Kochetkov, et al., *Earthquakes and Fundamentals of Seismic Zoning of Mongolia*, Ed. by V. P. Solonenko and N. A. Florensov (Nauka, Moscow, 1985) [in Russian].
38. S. S. Tsypukova, A. B. Perepelov, E. I. Demonterova, A. V. Ivanov, S. I. Dril', M. I. Kuzmin, A. V. Travin, Yu. D. Shcherbakov, M. Yu. Nuzankov, and S. V. Kanakin, "Two stages of the Cenozoic alkaline-basalt volcanism in the Darkhad Depression (Northern Mongolia)—Geochronology, Geochemistry, and Geodynamic Consequences," Geodynam. Tectonophys. **13** (3), 0613 (2022). https://doi.org/10.5800/GT-2022-13-3-0613
39. H. Çelik, Ya. I. Trikhunkov, S. A. Sokolov, V. G. Trifonov, E. A. Zelenin, Yu. Kargınoğlu, K. I. Yushin,

V. S. Lomov, and D. M. Bachmanov, "Tectonic aspects of the East Anatolian 06.02.2023 earthquake in Turkiye," Izv., Phys. Solid Earth **59**, 822–838 (2023).

40. A. V. Chipizubov and O. P. Smekalin, "Paleoseismodislocations and related paleoearthquakes along the Major Sayan Fault Zone," Geol. Geofiz. **40** (6), 936–947 (1999).
41. A. V. Chipizubov, O. P. Smekalin, and R. M. Semenov, "Fault scarps and prehistoric earthquakes in the Tunka Fault (southwestern Baikal Region)," Russ. Geol. Geophys. **44** (6), 561–574 (2003).
42. A. Arjannikova, C. Larroque, J.-F. Ritz, J. Deverchere, J.-F. Stephan, S. Arjannikov, and V. San'kov, "Geometry and kinematics of recent deformation in the Mondy–Tunka Area (south-westernmost Baikal Rift Zone, Mongolia–Siberia)," Terra Nova **16** (5), 265–272 (2004).
43. A. Arzhannikova, S. Arzhannikov, M. Jolivet, R. Vassallo, and A. Chauvet, "Pliocene to Quaternary deformation in South East Sayan (Siberia): Initiation of the Tertiary compressive phase in the southern termination of the Baikal Rift System," J. Asian Earth Sci. **40**, 581–594 (2011).
44. A. V. Arzhannikova, S. G. Arzhannikov, A. A. Chebotarev, and E. Nomin-Erdene, "Morphotectonics and Paleoseismology of the North Darhad Fault (SW Baikal Rift, Mongolia)," J. Asian Earth Sci **259**, Art.105882 (2024). https://doi.org/10.1016/j.jseaes.2023.105882
45. A. Arzhannikova, S. Arzhannikov, J.-F. Ritz, A. Chebotarev, and A. Yakhnenko, "Earthquake geology of the Mondy Fault (SW Baikal Rift, Siberia)," J. Asian Earth Sci. **248**, 105614 (2023). https://doi.org/10.1016/j.jseaes.2023.105614
46. I. Baljinnyam, A. Bayasgalan, B. A. Borisov, A. Cisternas, M. G. Dem'yanovich, L. Ganbataar, V. M. Kochetkov, R. A. Kurushin, P. Molnar, H. Philip, Yu. Ya. Vashchilov, *Ruptures of Major Earthquakes and Active Deformation in Mongolia and Its Surrounding* (USA, GSA Mem., 1993, Vol. 181).
47. D. Battogtokh, A. Bayasgalan, K. Wang, D. Ganzorig, J. Bayaraa, "The 2021 $M_w = 6.7$ Khankh earthquake in the Khuvsgul Rift, Mongolia," Mongolian Geoscientist **26** (52), 46–61 (2021).
48. C. Bronk Ramsey, "Bayesian analysis of radiocarbon dates," Radiocarbon **51** (1), 337–360 (2009).
49. A. Chebotarev, A. Arzhannikova, and S. Arzhannikov, "Long-term throw rates and landscape response to tectonic activity of the Tunka Fault (Baikal Rift) based on morphometry," Tectonophysics **810**, Art. 228864 (2021).
50. J.-H. Choi, Ya. Klinger, M. Ferry, J.-F. Ritz, R. Kurtz, M. Rizza, L. Bollinger, B. Davaasambuu, N. Tsend-Ayush, and S. Demberel, "Geologic inheritance and earthquake rupture processes: The 1905 $M \geq 8$ Tsetserleg-Bulnay strike-slip earthquake sequence, Mongolia," J. Geophys. Res.: Solid Earth **123** (2), 1925–1953 (2018).
51. *Database of Active Faults of Eurasia* (GIN RAS, Moscow, 2020). http://neotec.ginras.ru/ database.html (Accessed November 12, 2022).
52. B. Delouis, J. Déverchère, V. Melnikova, N. Radziminovitch, L. Loncke, C. Larroque, J. F. Ritz, and V. Sankov, "A reappraisal of the 1950 ($M_w = 6.9$) Mondy earthquake, Siberia, and its relationship to the strain pattern at the south-western end of the Baikal rift zone," Terra Nova **14**, 491–500 (2002).
53. R. Freund, "Kinematics of transform and transcurrent faults," Tectonophysics **21**, 93–134 (1974).
54. Hovsgol Drilling Project Members (A. A. Abzaeva, E. V. Bezrukova, V. A. Bychinsky, S. A. Fedenya, K. Fukishi, V. F. Geletyc, A. V. Goreglyad, E. V. Ivanov, G. V. Kalmychkov, K. Kashiwaya, T. Kawai, E. V. Kerber, M. Yu. Khomutova, G. K. Khursevich, J.-Y. Kim, M. A. Krainov, N. V. Kulagina, M. I. Kuzmin, P. P. Letunova, K. Minoura, W.-H. Nahm, Ts. Narantsetseg, Ts. Oyunchimeg, A. A. Prokopenko, H. Sakai, E. P. Solotchina, Y. Tani, L. L. Tkachenko, D. Tomurhuu, and T. Watanabe), "Sedimentary record from Lake Hovsgol, NW Mongolia: Results from the HDP-04 and HDP-06 drill cores," Quat. Int. **205** (1–2), 21–37 (2009). https://doi.org/10.1016/j.quaint.2009.02.008
55. C. Li, R. D. van der Hilst, E. R. Engdahl, and S. Burdick, "A new global model for P wave speed variations in Earth's mantle," Geochem. Geophys. Geosyst. **9** (5), 1–21 (2008).
56. X. Liu, W. Xu, N. A. Radziminovich, N. Fang, and L. Xie, "Transtensional coseismic fault slip of the 2021 M_w 6.7 Turt Earthquake and heterogeneous tectonic stress surrounding the Hovsgol Basin, Northwest Mongolia," Tectonophysics **836**, Art. 229407 (2022).
57. A. Orkhonselenge, S. K. Krivonogov, K. Mino, K. Kashiwaya, I. Y. Safonova, M. Yamamoto, K. Kashima, T. Nakamura, and J. Y. Kim, "Holocene sedimentary records from Lake Borsog, eastern shore of Lake Khuvsgul, Mongolia, and their paleoenvironmental implications," Quat. Int. **290–291**, 95–109 (2013). https://doi.org/10.1016/j.quaint.2012.03.041
58. S. V. Rasskazov, J. F. Luhr, S. A. Bowring, A. V. Ivanov, I. S. Brandt, S. B. Brandt, E. I. Demonterova, A. A. Boven, M. Kunk, T. Housh, and M. A. Dungan, "Late Cenozoic volcanism in the Baikal rift system: evidence for formation of the Baikal and Khubsugul basins due to thermal impacts on the lithosphere and collision-derived tectonic," Berliner Palaobiol. Abh. **4**, 33–48 (2003).
59. N. Radziminovich, G. Bayaraa, A. Miroshnichenko, S. Demberel, M. Ulziibat, D. Ganzorig, and A. Lukhnev, "Focal mechanisms of earthquakes and stress field of the crust in Mongolia and its surroundings," Geodynam. Tectonophys. **7** (1), 23–38 (2016). https://doi.org/10.5800/GT-2016-7-1-0195
60. P. J. Reimer, E. Bard, A. Bayliss, J. W. Beck, P. G. Blackwell, C. Bronk Ramsey, P. M. Grootes, T. P. Guilderson, H. Haflidason, I. Hajdas, C. HattŽ, T. J. Heaton, D. L. Hoffmann, A. G. Hogg, K. A. Hughen, K. F. Kaiser, B. Kromer, S. W. Manning, M. Niu, R. W. Reimer, D. A. Richards, E. M. Scott, J. R. Southon, R. A. Staff, C. S. M. Turney, and J. van der Plicht, "IntCal13 and Marine13 radiocarbon age calibration curves 0-50 000 Years Cal BP," Radiocarbon **55** (4), 1869–1887 (2013).
61. P. J. Reimer, W. E. N. Austin, E. Bard, A. Bayliss, J. W. Beck, P. G. Blackwell, C. Bronk Ramsey, M. Butzin, H. Cheng, R. L. Edward, M. Friedrich, P. M. Grootes, T. P. Guilderson, I. Hajdas, T. J. Heaton, A. G. Hogg,

K. A. Hughen, B. Kromer, S. W. Manning, R. Muscheler, J. G. Palmer, C. Pearson, R. W. Reimer, D. A. Richards, E. M. Scott, J. R. Southon, C. S. Turney, J. van der Plicht, L. Wacker, F. Adolphi, U. Büntgen, M. Capano, S. M. Fahrni, V. M. Fogtmann-Schmidt, A. Schulz, R. Friedrich, P. Köhler, S. Kudsk, F. Miyake, J. Olsen, F. Reinig, M. Sakamoto, A. Sookdeo, and S. Talamo, "The IntCal20 Northern Hemisphere radiocarbon age calibration curve (0–55 cal kBP)," Radiocarbon **62** (4), 725–757 (2020).

62. J.-F. Ritz, A. Arzhannikova, R. Vassallo, S. Arzhannikov, C. Larroque, J.-L. Michelot, and M. Massault, "Characterizing the present-day activity of the Tunka and Sayan faults within their relay zone (western Baikal rift system, Russia)," Tectonics **37**, 1376–1392 (2018).
63. M. Rizza, J.-F. Ritz, C. Prentice, R. Vassallo, R. Braucher, C. Larroque, A. Arzhannikova, S. Arzhannikov, S. Mahan, M. Massault, J.-L. Michelot, and M. Todbileg, "Earthquake geology of the Bolnay Fault (Mongolia)," Seismol. Soc. Am. Bull. **105** (1), 72–93 (2015).
64. A. Schlupp and A. Cisternas, "Source history of the 1905 great Mongolian earthquakes (Tsetserleg, Bolnay)," Geophys. J. Int. **169** (3), 1115–1131 (2007).
65. A. A. Shchetnikov, D. White, I. A. Filinov, and N. Rutter, "Late Quaternary geology of the Tunka rift basin (Lake Baikal region), Russia," J. Asian Earth Sci. **46**, 195–208 (2012).
66. V. G. Trifonov, A. M. Korzhenkov, and Kh. M. Omar, "Recent geodynamics of major strike-slip zones," Geodes. Geodynam. **6** (5), 361–383 (2015).
67. R. E. Wallace, "Note on stream channels offset by the San Andreas fault, southern Coast Ranges, California," in *Proc. Conf. "Geological Problems of San Andreas Fault System"* (Stanford Univ. Publ. Geol. Sci., Stanford, USA, 1968, Vol. 11), pp. 6–20.
68. *Catalog of Earthquakes of the United Geophysical Center of RAS*. http://www.ceme.gsras.ru (Accessed November 10, 2023).

Translated by D. Voroshchuk